Optimal intensity measures for the structural assessment of buried steel natural gas pipelines due to seismically-induced axial compression at geotechnical discontinuities

Grigorios Tsinidis[1], Luigi Di Sarno[2], Anastasios Sextos[3], and Peter Furtner[4]

[1]Vienna Consulting Engineers ZT GmbH, Austria & University of Sannio, Italy
[2] University of Liverpool, United Kingdom & University of Sannio, Italy
[3]University of Bristol, United Kingdom
[4]Vienna Consulting Engineers ZT GmbH, Austria

Corresponding Author: Dr Grigorios Tsinidis, VCE Vienna Consulting Engineers ZT GmbH, Untere Viaduktgasse 2, 1030, Vienna, email: tsinidis.grigorios@gmail.com

Abstract: This paper investigates the efficiency and sufficiency of various seismic intensity measures for the structural assessment of buried steel natural gas (NG) pipelines subjected to axial compression caused by transient seismic ground deformations. The study focuses on buried NG pipelines crossing perpendicularly a vertical geotechnical discontinuity with an abrupt change on the soil properties, where the potential of high compression strain is expected to be increased under seismic wave propagation. A detailed analytical framework is developed for this purpose, which includes a 3D finite element model of the pipe-trench system, to evaluate rigorously the pipe-soil interaction phenomena, and 1D soil response analyses that are employed to determine critical ground deformation patterns at the geotechnical discontinuity, caused by seismic wave propagation. A comprehensive numerical parametric study is conducted by employing the analytical methodology in a number of soil-pipeline configurations, considering salient parameters that control the axial response of buried steel NG pipelines, i.e. diameter, wall thickness and internal pressure of the pipeline, wall imperfections of the pipeline, soil properties and backfill compaction level and friction characteristics of the backfill-pipe interface. Using the peak compression strain of the pipeline as engineering demand parameter and a number of regression analyses relative to the examined seismic intensity measures, it is shown that the peak ground velocity *PGV* at ground surface constitutes the optimum intensity measure for the structural assessment of the examined infrastructure.

Keywords: Natural gas pipelines; intensity measures; efficiency; sufficiency; steel pipelines; local buckling

1. Introduction

Earthquake-induced damage on Natural Gas (NG) pipeline networks may lead to important direct and indirect economic losses. The 1999 Chi-Chi earthquake in Taiwan, for instance, caused noticeable damage on natural gas supply systems, with the associated economic loss for the relative industry exceeding $ 25 million [1, 2]. More importantly, severe damage may trigger ignitions or explosions with life-treating consequences and significant effects on the environment. As an example, the 1995 Hyogo-Ken Nambu earthquake in Japan, caused gas leakages from buried pipelines at 234 different locations, which subsequently led to more than 530 fires [3, 4]. Based on the above observations, efficient methods for the vulnerability assessment of NG pipeline networks seem to be of great importance.

A critical step towards the development of adequate tools for the vulnerability assessment of NG pipelines is the identification of the expected failures, as well as of the mechanisms that lead to these failures. Post-earthquake observations have demonstrated that seismically-induced ground deformations may induce significant damage on buried pipelines [5-8]. Buried steel NG pipelines were found quite vulnerable to high straining imposed by permanent ground deformations, associated with fault movements, landslides and liquefaction-induced settlements or uplifting and lateral spreading [5]. Seismically-induced transient ground deformations, caused by seismic wave propagation, have also contributed to damage of this infrastructure [9-11]. Permanent ground deformations tend to induce higher straining on buried steel pipelines, compared to transient ground deformations. Hence, most researchers focused their investigations on this seismic hazard [12-23]. However, it is more likely for a buried pipeline to be subjected to transient ground deformations rather than seismically-induced permanent ground deformations. Transient ground deformations may trigger a variety of damage modes on continuous buried steel NG pipelines, such as: shell-mode buckling or local buckling, beam-mode buckling, pure tensile rupture, flexural bending failure or excessive deformation of the section (i.e. ovaling) [5]. Additionally, recent studies have demonstrated that pipelines embedded in heterogeneous sites or subjected to asynchronous seismic motion are more likely to be affected by appreciable strains due to transient ground deformations, which in turn may lead to exceedance of predefined performance limits, reaching even excessive damage on the pipeline [24-25]. Based on the above considerations, the present study focuses on the transient ground deformation effects, as these have not yet been studied in adequate depth.

An important aspect for the integrity assessment of NG pipeline networks is the aleatory and epistemic uncertainty that is associated with their seismic response and vulnerability. In fact, a shift from conventional deterministic analysis procedures to probabilistic analysis and risk assessment concepts is deemed necessary [24]. Critical elements of the latter analysis frameworks are: (i) the definition of a proper Engineering Demand Parameter (*EDP*), which shall be used as a representative metric of the response of the examined element at risk, and (ii) the identification of adequate seismic intensity measures (*IMs*), which shall express the severity of the ground seismic motion [26].

Evidently, the amplitude, frequency characteristics, energy content and duration of seismic ground motions are all expected to have a considerable effect on the seismic vulnerability of

any structural element at risk. However, it is not possible for all the above ground motion characteristics to be described effectively by one parameter, i.e. one seismic intensity measure (*IM*) [26]. Therefore, the definition of *optimal seismic IMs* for the assessment of any structural system is of great importance. An *optimal* seismic *IM* should be *efficient*, in the sense that it should result in a reduced variability of the *EDP* for a given *IM* value [27]. Additionally, it should be *sufficient*, so that it renders the computed structural response conditionally independent of earthquake characteristics, such as the earthquake magnitude (*M*), the epicentral distance (*R*) or other earthquake characteristics [28]. An efficient seismic *IM* leads to a reduction of the number of analyses and ground seismic motions that are required to estimate the probability of exceedance of each value of the *EDP* for a given *IM* value. A sufficient *IM*, on the other hand, allows for free selection of the, employed in the analysis, seismic ground motions since the effects of seismological parameters, e.g. the magnitude, epicentral distance etc., on the prediction of the *EDP* become less important. As discussed in the ensuing, the efficiency and sufficiency of a seismic *IM* may be both quantified following existing literature [28-29].

Concepts and measures like *proficiency, practicality, effectiveness, robustness* and *hazard computability*, have also been proposed in the literature for identifying optimal seismic *IMs* for the assessment of buildings and aboveground civil infrastructure [27-36, 86-87]. However, the investigation of optimal seismic *IMs* for embedded infrastructure, including buried steel NG pipelines, has received considerably less attention by the scientific community. To the authors' knowledge, the only relevant study is the one by Shakid & Jahangiri [37], who developed and employed a numerical framework, in order to examine the efficiency and sufficiency of a variety of seismic *IMs* in case of NG pipelines subjected to seismic wave propagation. The study focused on NG pipelines embedded in uniform soils, with the soil-pipe interaction being considered in a simplified fashion, by employing beam on soil-springs models. The researchers did not examine a variety of parameters affecting the seismic response and vulnerability of this infrastructure.

Based on the above considerations, the aim of this study is to identify the optimum seismic *IMs* that shall be adopted for the assessment of buried steel natural gas (NG) pipelines, when these are subjected to compression axial loading due to transient seismic ground deformations. The study focuses on NG pipelines crossing perpendicularly a vertical geotechnical discontinuity with an abrupt change on the soil properties. In such soil sites, the potential of high compression straining of the pipeline during ground shaking is expected to increase significantly, compared to the case where the pipeline is embedded in a homogeneous soil site [24-25]. A de-coupled numerical framework is developed to fulfil our objective, which includes 1D soil response analyses of selected soil sites and 3D quasi-static analyses of selected soil-pipe configurations. The former analyses aim at computing critical ground deformation patterns at the vicinity of the geotechnical discontinuity, caused by seismic wave propagation. Through the 3D soil-pipe interaction analyses, critical parameters affecting the seismic response and vulnerability of buried steel pipelines are thoroughly considered. A comprehensive study is conducted for an ensemble of 40 seismic motions, by employing the proposed numerical methodology in a number of soil-pipe configurations. Various seismic

IMs, referring to both outcrop and ground surface conditions, are tested and rated on the basis of two criteria namely their *efficiency* and *sufficiency* [27-28].

2. Numerical parametric analysis

2.1 Problem definition and selection of soil-pipe configurations

A continuous buried steel NG pipeline of external diameter D and wall thickness t is embedded in a backfilled trench at a burial depth h (Fig. 1). The backfill-pipe configuration is located in a soil deposit of total depth H and crosses perpendicularly a vertical geotechnical discontinuity. The latter divides the soil deposit into two subdeposits (i.e. subdeposit 1 and subdeposit 2 in Fig. 1) with abrupt changes on their physical and mechanical properties. The whole system is subjected to upward propagated seismic shear waves, which cause a dissimilar ground movement of the adjusted subdeposits. The dissimilar ground movement of the subdeposits produces a differential horizontal ground deformation along the pipeline axis near the critical section of the geotechnical discontinuity. This differential ground deformation is subsequently transferred through the pipe-soil interface on the pipeline, causing its compressional-tensional axial straining. A potential high axial compression straining of the pipeline might lead to a failure of the pipeline in the form of local buckling.
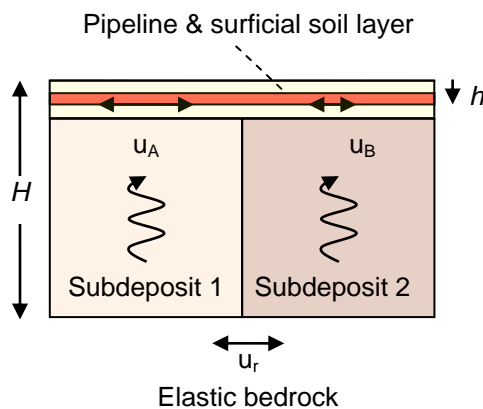
Fig. 1 Schematic view of the examined problem (H: depth of soil deposit, h: burial depth of the pipeline, u_r: seismic ground movement of the bedrock, u_A, u_B seismic ground movement of subdeposit 1 and 2, at the burial depth of the pipeline).

A number of parameters affecting the seismic response of buried steel pipelines namely wall thickness, diameter, and burial depth of the pipeline, internal pressure of the pipeline, existence of wall imperfections of the pipeline, backfill compaction level, pipe-backfill interface friction characteristics and soil properties of the site, are all considered in the present numerical study. In particular, most analyses were carried out on pipelines with external diameter $D = 914.4$ mm and wall thickness $t = 12.7$ m, while additional analyses were conducted for pipelines with external diameters $D = 406.4$ mm and $D = 1219.2$ mm and wall thicknesses $t = 9.5$ mm and $t = 19.1$ mm, respectively. The selected pipelines were designed for a maximum operational pressure of $p = 9$ MPa (i.e. 90 bar), following relevant regulations of ALA (2001) [38], while it was verified that the selected pipeline dimensions are available by the industry. Most of analyses were conducted for an operational pressure, $p = 8$ MPa, while sensitivity analyses

were also carried out for an internal pressure p = 4 MPa, as well as for non-pressurized pipelines (i.e. p = 0 MPa). It is worth noticing that the external diameters, D, and operational pressures, p, of the investigated pipelines were all selected on the basis of a preliminary investigation of the variation of these characteristics in case of actual transmission NG networks found in several countries of Europe (Table 1). The external diameter, wall thickness and examined internal pressures of the selected pipelines are summarized in Table 2. The pipelines were assumed to be made of API 5L X60, X65 and X70 grades, in an effort to cover a range of steel grades that are commonly used in NG transmission networks. The mechanical properties of the selected grades are tabulated in Table 3.

Table 1 External diameters and range of operational pressure of transmission NG pipeline networks in Europe (information provided by the website of each operator).

Country	Operator	Nominal diameter range, D (mm, ')	Operational pressure range, p (MPa)
Austria	TAG	914.4 mm to 1066.8 mm (36' to 42')	7 - 8
Belgium	Fluxys Belgium	914.4 mm, 965.2 mm, 1016.0 mm (36', 38', 40')	4 - 7
Germany	Gascade	> 1066.8 mm (42') for the supra-regional networks; otherwise > 508 mm to 762 mm (20' to 30')	*n.p.**
Germany	Gasunie	> 1066.8 mm (42') for the supra-regional networks; otherwise > 508 mm to 762 mm (20' to 30')	*n.p.*
Greece	DESFA	254 mm, 508 mm, 609.6 mm, 762 mm, 914.4 mm (10', 20', 24', 30', 36')	7
Italy	SNAM	508 mm to 1219.2 mm (20' to 48')	7 - 8
Spain	Enegas	406.4 mm to 812.8 mm (16' to 32')	*n.p.*
Sweden	Swedegas	406.4 mm to 660.4 mm (16' to 26')	5 - 8
Switzerland	Transitgas	914.4 mm to 1066.8 mm (36' to 48')	7 - 8

* n.p. = not provided

Table 2 Summary of examined cases.

External diameter, D (')	External diameter, D (mm)	Wall thickness, t (mm)	D/t	Internal pressure, p (MPa)	Burial depth, h (m)	Depth of soil sites, H (m)	Surficial soil-trench properties
16'	406.4	9.5	42.8	8	1.0	60	TA, TB
36'	914.4	12.7	72.0	0, 4, 8	1.0, 2.0	30,60,120	TA, TB
48'	1219.2	19.1	63.8	8	1.0	60	TA, TB

Table 3 Mechanical properties of steel grades used in this study.

Steel grade	X60	X65	X70
Yield stress, σ_y (MPa)	414	448	483
Ultimate stress, σ_u (MPa)	517	531	565
Ultimate tensile strain, ε_u (%)	14.2	13	11.2
Young's modulus, E (GPa)	210	210	210

The study was conducted assuming a soil site depth H = 60 m, while additional analyses were also carried out for soil sites with depths equal to 30 m and 120 m. The burial depth, h, of the

1   selected pipelines, i.e. distance between the pipeline crown and ground surface, was set equal

2   to 1.0 m, which constitutes a common burial depth for this infrastructure. A sensitivity study

3   was conducted for $D = 914.4$ mm pipelines buried at a burial depth $h = 2.0$ m.

4   Both cohesive and cohesionless soil deposits were examined, with the properties of the

5   examined pairs of subdeposits varying so that to cover a range of anticipated soil sites. A 3.0 m

6   deep surficial layer of cohesionless material was assumed in all examined cases, regardless of

7   the adopted underlying subdeposits. Additionally, all examined sites were assumed to rest on

8   an elastic bedrock with mass density, $\rho_b = 2.2$ t/m^3 and shear wave velocity $V_{s,b} = 1000$ m/s.

9   Fig. 2 illustrates the gradients of shear wave propagation velocities, as well as the mass

10   densities, ρ, of the selected soil subdeposits. The variation of the small-strain shear modulus of

11   the cohesionless subdeposits was actually estimated as follows [39]:

12
$$G_{\max} = 220 K_{2,\max} \left(\sigma'_m \right)^{0.5} \qquad (1)$$
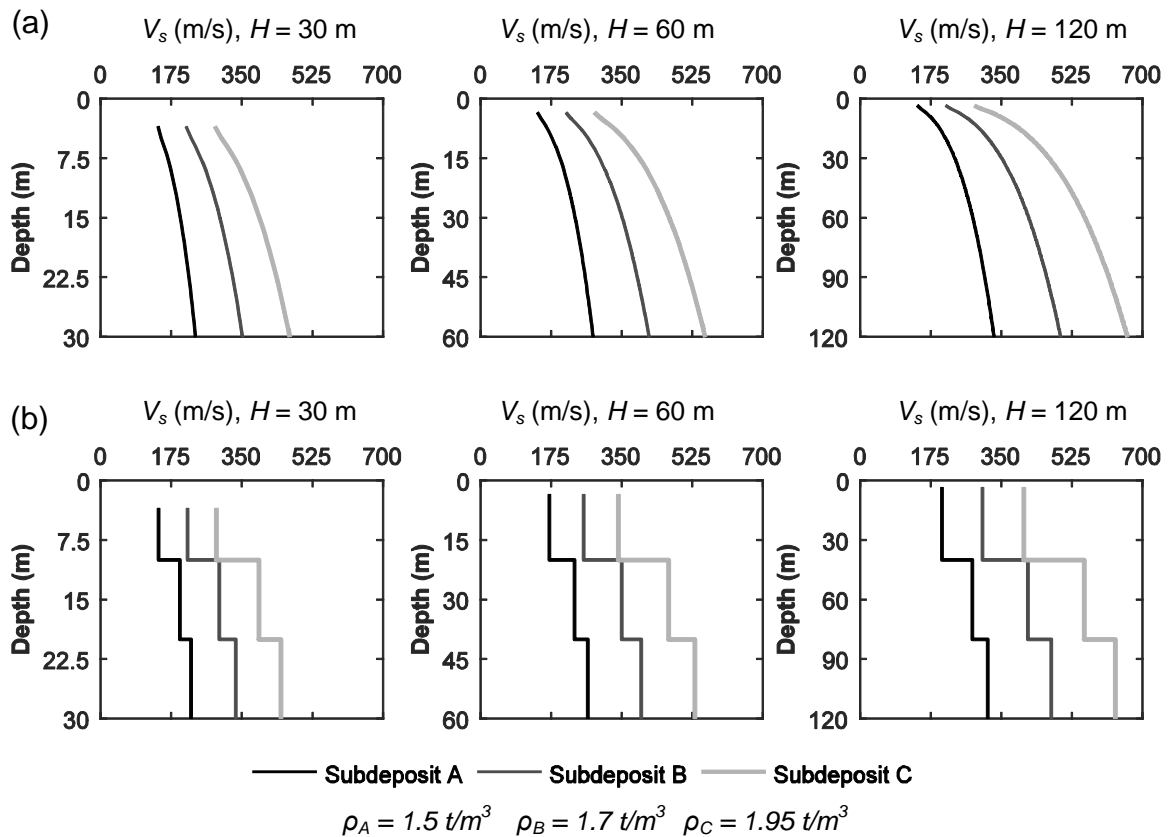
Fig. 2 Shear wave velocity gradients of examined (a) cohesionless and (b) cohesive soil sub-deposits.

16   where σ'_m is the effective confining stress (in kPa) and $K_{2,\max}$ is a constant depending on the

17   relative stiffness D_r of the subdeposit (Table 4). By employing Eq. 1 for the selected soil mass

18   densities and based on basic elasto-dynamics, the gradients of small-strain shear wave velocity

19   were defined, as per Fig. 2a. The gradients of the small-strain shear wave velocity of the

20   cohesive soil subdeposits were also considered to be increased with depth, as per Fig. 2b. The

21   selected soil subdeposits correspond to soil classes B and C according to Eurocode 8 [40]. The

22   above profiles were selected in pairs, in order to define the properties of subdeposits 1 and 2

23   (Fig. 1). In particular, three pairs were examined, i.e. Soil A - Soil B, Soil A - Soil C and Soil

B - Soil C. The nonlinear response of the selected subdeposits during ground seismic shaking was described by means of G-γ-D curves, following [41].

Two different sets of mechanical and physical properties were examined for the surficial soil layer, which actually constitutes the trench backfill material for the examined pipelines and therefore is referred as either *trench TA* or *trench TB* in the ensuing, for the sake of simplicity. The selected properties, summarized in Table 5, correspond to well or very well-compacted conditions. It is worth noting that the shear moduli G, presented in Table 5, correspond to 'average' equivalent soil stiffnesses, referring to the ground strain range anticipated for the selected seismic ground motions. These values were estimated on the basis of nonlinear 1D soil response analyses, discussed in the following.

With reference to the selection of the friction coefficient of the backfill-pipe interface, μ; this may vary along the axis of a long pipeline and may also change during ground shaking. However, for steel pipelines without external coating, it is bounded between $\mu_{min} = 0.3$ and $\mu_{max} = 0.8$. These limits are resulted from the relation between the interface friction coefficient μ and friction angle of the backfill φ, i.e. $\mu = (0.5 - 0.9) \times \tan\varphi$ [38, 42], by assuming typical values for the backfill soil friction angle, i.e. from 29° to 44°. It is worth noting that the existence of external pipe coating may affect the friction coefficient of the interface [38]. This effect was disregarded in this study, since the focus was set on more critical cases where higher shear stresses are developed along the pipe-soil interface, leading to a higher axial straining on the embedded pipeline.

Table 4 Relationships between density, relative density, $K_{2,max}$ parameter and cohesionless soil characterization (after [39]).

Density, ρ (t/m^3)	Relative density, D_r (%)	$K_{2,max}$	Characterization
1.4	30	30	Loose
1.65	52.5	48	Medium
2	90	70	Fine

Table 5 Physical and mechanical properties of investigated trenches.

|	Density, ρ (t/m^3)	Poisson's ratio, v	Shear modulus, G (MPa)	Friction angle, φ ($^{\circ}$)	Friction coefficient, μ
Trench TA	1.65	0.3	37.1	35	0.45
Trench TB	1.9	0.3	63.1	44	0.78

2.2 Analytical methodology

A 3D full dynamic analysis of the soil-pipe interaction (SPI) phenomena during ground shaking may be seen as computationally prohibitive, when considering the complications in simulating rigorously material or geometrical nonlinearities associated with the problem, as well as the uncertainties in the definition of the characteristics of heterogeneous soil sites and the inherently random varying ground seismic motion [25]. Hence, a simplified, yet efficient, numerical analysis framework should be developed and used, instead.

Generally, the inertial soil-structure interaction (SSI) effects are not important in the dynamic soil-pipe interaction problem [42]. This allows for a decoupling of the problem in successive stages, in an effort to reduce the computational cost compared to the one associated with a 3D SPI dynamic analysis. It also allows for the investigation of the effect of transient ground deformation on the response of the embedded pipeline in a quasi-static form.

Based on the above considerations, a numerical framework was developed within this study. The framework, which is inspired by Psyrras et al. [25], is illustrated schematically in Fig. 3 and consists of three main steps. A 3D trench-pipe numerical model is constructed within the first step to compute the axial compressive response of the buried steel NG pipeline under an increasing level of relative axial ground displacement, caused by the dissimilar ground movement of adjacent soil subdeposits near the geotechnical discontinuity (Step 1 in Fig. 3). In the second step (Step 2 in Fig. 3), the ground response is computed under vertically propagated seismic waves via 1D nonlinear soil response analyses, which are carried out separately for each subdeposit. More specifically, critical relative axial ground deformation patterns, δ_{ue}, are computed at the pipeline depth, for the selected pairs of subdeposits, using the numerically predicted horizontal deformations of the adjacent soil subdeposits. Time histories of acceleration, velocity and displacement are also computed at the ground surface, which are then employed in the definition of some of the examined seismic *IMs* in the present study. The outcomes of the 3D SPI analyses and the 1D soil response analyses are combined in the third step of the analytical framework (Step 3 in Fig. 3). In particular, the pipe response, expressed in terms of maximum axial compression strain, is correlated with the ground response, the latter computed for each of the selected pairs of subdeposits and each seismic record. The analytical framework is further analysed in the following sections.
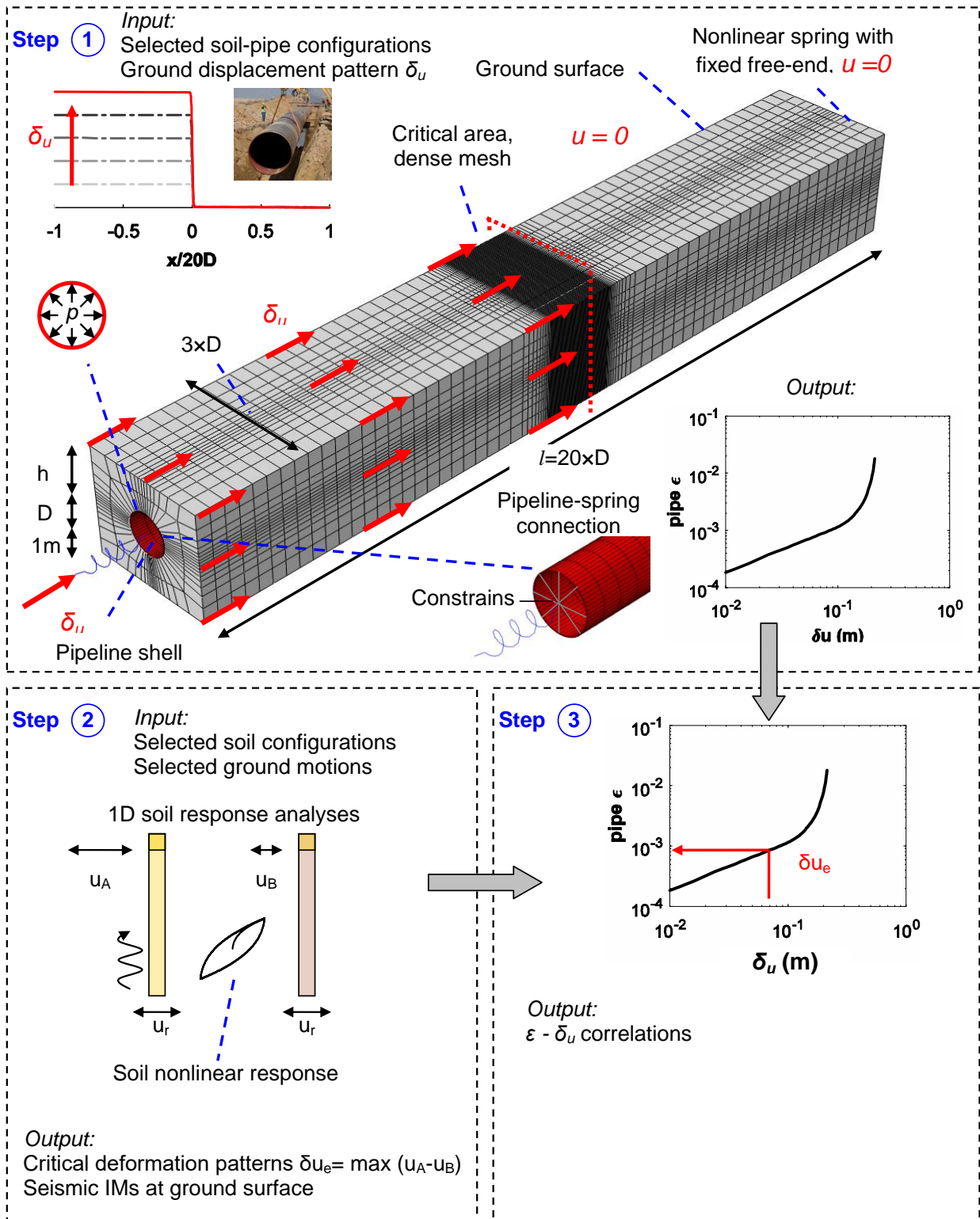
Fig. 3 Schematic view of the analysis framework: Step 1: 3D numerical model of the trench-pipe configuration to evaluate the pipeline response under an increasing level of relative axial ground deformations, δ_u, accounting for the SPI effects. Step 2: 1D soil response analyses of selected soil subdeposits to compute the ground response for selected ground motions, including the seismic *IMs* at ground surface, and define relative axial ground deformations δ_{ue}, at the vicinity of the geotechnical discontinuity. Step 3: combination of the results of the 3D SPI analyses with the results of the 1D soil response analyses.

2.2.1 Step 1: 3D trench-pipe model to analyse the SPI phenomena

A 3D continuum trench model, encasing a cylindrical shell model of the pipeline, is initially developed in ABAQUS [43], aiming at computing the axial response of the pipeline under an increasing level of relative axial ground displacement, caused by the dissimilar horizontal ground shaking of the adjacent subdeposits near a geotechnical discontinuity (Step 1 in Fig. 3). The utilization of a 3D continuum model allows for a rigorous simulation of pressurization level of the pipeline, as well as of initial geometric imperfections of the wall of the pipeline, which both are expected to affect significantly the axial compressional response of a buried steel pipeline, including potential localized buckling modes [24, 45-48]. Additionally, it allows for a rigorous simulation of potential sliding and/or detachment (i.e. in the normal direction) of the pipeline wall from the surrounding ground, by employing interaction models available in advanced finite element codes, like ABAQUS [43]. Finally, it allows for a proper simulation of the initial stress state and deformation of the trench-pipe system, caused by gravity and the operational pressure of the pipeline, before the application of the seismically-induced ground deformations.

The selection of a surficial block from the semi-infinite 3D ground domain, i.e. a part of the surficial layer-trench TA or TB herein, is made on the ground of absence of significant inertial SSI effects, in addition to the shallow burial depth of the pipeline and the assumption of in-plane ground deformation pattern. In this context, the dimensions of the 3D model are defined as follows; the distance between the pipe invert and the bottom boundary of the trench model is set equal to 1.0 m, while the distance between the side boundaries of the trench model and the pipe edges is set equal to one pipe diameter. The distance between the pipe crown and ground surface is defined according to the adopted burial depth, h, of the examined pipeline.

An 'adequately long' 3D continuum model is generally required to account for the effect of the 'anchorage' length of the pipeline by the surrounding ground on the shear stresses that are being developed along the soil-pipe interface during seismic ground deformation. This aspect in addition to the requirement of fine meshes of the pipeline, to adequately resolve its buckling modes (see following), may lead to a significant increase of the relevant computational cost of the analyses, even if these analyses are conducted in a quasi-static fashion. On this basis, generalized nonlinear springs are calculated and introduced at both sides of the pipeline, in an effort to reduce the required length of the 3D SPI model, while considering the effect of the 'infinite' pipeline length on the response of the examined pipeline-soil configurations. The springs are acting parallel to the pipeline axis, with the force-displacement relation of the nonlinear springs being given as follows [24]:

$$F = \begin{cases} \lambda EA\delta_x & \text{for} \quad \delta_x \leq \dfrac{\tau_{max}}{k_s} \\[2em] \lambda EA\dfrac{\tau_{max}}{k_s} + \dfrac{\pi D\tau_{max}}{m}\left(\sqrt{\left(\lambda\dfrac{\tau_{max}}{k_s}\right)^2 + 2m\left(\delta_x - \dfrac{\tau_{max}}{k_s}\right)} - \left(\lambda\dfrac{\tau_{max}}{k_s}\right)\right) & \text{for} \quad \delta_x > \dfrac{\tau_{max}}{k_s} \end{cases} \tag{2}$$

where:

$$\lambda = \sqrt{\frac{\pi D k_s}{EA}} \qquad (3)$$

$$m = \frac{\pi D \tau_{max}}{EA} \qquad (4)$$

δ_x is the backfill-pipe relative axial movement caused by the relative axial ground deformation δ_u of the trench backfill soil, as a result of the dissimilar ground movement of the adjacent sub-deposits, k_s is the shear stiffness of the backfill-pipe interface, τ_{max} is the maximum shear resistance that develops along the backfill-pipe interface and *EA* is the axial stiffness of the pipeline cross section. The maximum shear resistance in case of cohesionless backfills depends on the adopted friction coefficient μ of the interface and varies along the perimeter of the pipe. Therefore, mean values of τ_{max} and k_s should be evaluated via numerical simulations of simple axial pull-out tests of the examined pipe from the trench backfill soil, as per [16]. The proposed simulation of the end-boundaries of the pipeline is inspired from a numerical model that was developed by Vazouras et al. [16] to account for the effect of the infinite length of a buried steel pipeline subjected to seismically-induced strike-slip faulting. Based on the above considerations, the length of the 3D pipe-soil trench model is reduced to $20 \times D$ (*D*: external diameter of the pipeline). This length is selected on the grounds of a sensitivity analysis, by comparing the axial stresses and strains computed at the critical middle section of the pipeline by the 3D SPI model, with relevant predictions of equivalent extended, almost 'infinite', 3D continuum models of the soil-pipe configuration, subjected to the same axial ground deformation pattern, as the one used for the hybrid 3D model with the springs at the pipe sides. The boundary at the bottom of the soil model is fixed in the vertical direction, whereas the side-boundaries are fixed in the horizontal direction. The ground surface is set free, while the pipe-ends are connected to the relevant springs by means of rigid constraints, as per Fig. 3a.

The backfill-pipe interface is simulated using an advanced 'hard contact' interaction model, available in ABAQUS [43], which allows for potential sliding and/or detachment (in the normal direction) between the interacting pipe and backfill soil elements during the horizontal deformation of the ground. The shear behaviour of the interface model is simulated via the classical Coulomb friction model, by introducing a friction coefficient, μ. The latter follows the values provided in Table 5.

A critical aspect for the efficiency of the 3D numerical model is the discretization of the pipeline and surrounding soil. Linear hexahedral (brick-type) elements are used to model the trench backfill, employing the equivalent soil properties (i.e. degraded soil stiffness) presented in Table 5. The pipeline is simulated by means of inelastic, reduced integration S4R shell elements, having both membrane and bending stiffness. The mesh density of the pipeline at the critical central section of the 3D numerical model, i.e. at the location of the geotechnical discontinuity where the axial strain of the pipeline is expected to maximize, is selected adequately, in order to resolve the inelastic buckling modes of an equivalent axially compressed unconstrained cylindrical steel shell [25]. To select an adequate mesh, the half-wavelength of the examined pipeline sections in the post-elastic range, $\lambda_{c,p}$, is initially computed as [49]:

1 $$\lambda_{c,p} \approx \lambda_{c,el} \times \sqrt{E_p/E} \qquad (5)$$

2 where E is the Young's modulus of the steel grade of the pipeline, E_p is the plastic modulus of

3 the steel grade of the pipeline and $\lambda_{c,el}$ the elastic axial half-wavelength. Considering a

4 Poisson's ratio $v = 0.3$ for the steel grades examined herein, the latter is given as [49]:

5 $$\lambda_{c,el} \approx 1.72\sqrt{Rt} \qquad (6)$$

6 where R and t are the radius and wall thickness of the pipeline, respectively. By setting the

7 plastic modulus E_p is equal to $0.1E$, Eq. 5 yields: $\lambda_{c,p} \approx 0.5\lambda_{c,e}$ [25]. Element lengths, ranging

8 between 1.0 cm and 2.0 cm, were found capable to reproduce the theoretical axial half-

9 wavelength $\lambda_{c,p}$ of the examined pipelines. The above mesh seeds are applied in the middle

10 section of the examined pipelines and for a length equal to 2.0 m. The mesh density away from

11 the critical central zone is gradually decreased, with the axial dimension of the shell elements

12 being as high as 0.30 m, to reduce the computation cost of the 3D analyses. This was done on

13 the ground of the small strain amplitudes and radial deflections expected away from the central

14 section of the pipeline. The mesh discretization of the trench soil in the axial direction of the

15 model matches the exact mesh seed of the pipeline, to avoid any initial gaps during the

16 generation of mesh. The mesh seed of the trench in the other two directions is restricted to 0.3

17 m.

18 The plastic behaviour of the steel pipelines is modelled through a classical J2-flow plasticity

19 model combined with a von Mises yield criterion. Ramberg-Osgood curves (Eq. 7) are fitted to

20 bilinear isotropic curves that describe the tensile uniaxial behaviour of the selected steel grades

21 (Fig. 4). The curves are characterized by a yield offset equal to 0.5 %, and a hardening

22 exponent n equal to 15, 19.5 and 21, for grades X60, X65 and X70, respectively.

23 $$\varepsilon = \frac{\sigma}{E} + a \times \left(\frac{\sigma}{\sigma_y}\right)^n \qquad (7)$$

24
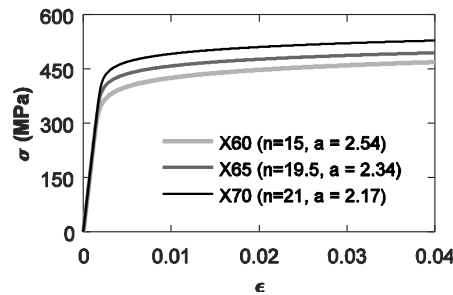
25
26 **Fig. 4** Uniaxial tensile stress-strain response of API X60, X65 and X70 steel grades adopted herein ($n =$
27 hardening exponent, $a =$ yield offset $\times E/\sigma_y$).

28

29 The axial compression response of thin-walled steel pipelines is known to be highly affected

30 by initial geometric imperfections of the walls [25, 44]. In this context, both 'perfect' pipelines

31 and equivalent pipelines with initial geometric imperfections of their walls are examined. The

32 simulation of imperfections of the pipeline walls is not a straightforward task since the shape of

33 these imperfections might be rather complex. In this study, a 'fictious' imperfection shape is

1 considered, following previous studies [25, 45]. In particular, a stress-free, biased
2 axisymmetric imperfection is considered, following a sinusoid function modulated by a second
3 sinusoid, which results in a peak amplitude of the imperfection at the middle section of the
4 length, where it is applied [25]. The function of radial deflection is defined as per Eq. (8),
5 where positive values correspond to outward direction form the mid-surface of the pipeline
6 shell wall.

7

8 $$\bar{w}(x) = \left[w_0 + w_1 \cos\left(\frac{\pi x}{N\lambda_c}\right) \right] \cos\left(\frac{\pi x}{\lambda_c}\right), \quad -\frac{L_{crit}}{2} \leq x \leq \frac{L_{crit}}{2}, \quad L_{crit} = 2.0m, \quad 2N\lambda_c = L_{crit} \qquad (8)$$

9
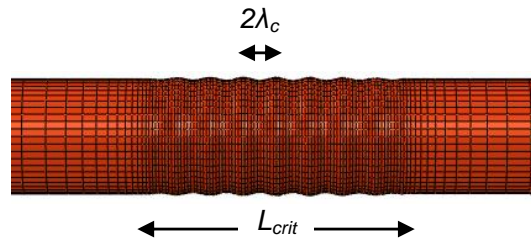
10
11 **Fig. 5** Detail of the mesh of the central section of a $D = 914.4$ mm pipeline with a biased axisymmetric
12 geometrical imperfection (the radial deformation is exaggerated by a scale factor of 10, × 10).

13

14 The peak amplitude of the imperfection is set as a function of the pipe wall thickness:
15 $w = w_0 + w_1 = 0.10t$. This latter selection is made following specifications, of ArcelorMittal
16 which provide a manufacturing tolerance for the walls of API-5L X65 pipelines in the range of
17 + 15% to -12.5% [50]. Generally, the location of a pipeline imperfection is not easily
18 detectable. In the present study it was decided to select the worst-case scenario, i.e. the
19 imperfection is applied over the central critical pipeline zone with length equal to $L_{crit} = 2.0$ m,
20 centered at the exact position of the geotechnical discontinuity. Fig. 5 illustrates a detail of the
21 mesh of the central section of an imperfect pipeline. The mesh of the backfill soil, surrounding
22 the pipeline, follows the perturbated mesh of the pipeline, in order to prevent any initial gaps
23 during the generation of the mesh that might affect the contact phenomena during loading, thus
24 decreasing the computational efficiency of the model. Residual stresses due to manufacturing
25 process of the pipelines were disregarded by the present study.
26 With reference to the loading pattern of the 3D SPI model; the effects of gravity and internal
27 pressure of the pipeline are initially considered within a general static step. The effect of
28 transient ground deformation is then simulated in quasi-static manner as follows: the nodes of
29 the one half of the trench model and the free node of the relevant nonlinear spring are fixed in
30 the axial direction, i.e. $u = 0$, in Fig. 3. The nodes of the other half trench model and the free
31 node of the relevant nonlinear spring are displaced towards the constraint part of the model in a
32 stepwise fashion. This deformation pattern causes a relative axial deformation of the backfill
33 model (i.e. δ_u), which is equivalent to the case where both halves of the model, are moving
34 differently but in the same axial direction, causing the same differential ground displacement δ_u
35 on the examined system. Since the depth of the trench domain is much smaller than the
36 common predominant wavelengths of shear seismic waves, the above-described deformation

pattern is kept constant with depth coordinate over the trench backfill domain. The adopted deformation pattern leads to the development of shear stresses along the pipe-soil interface, which in addition to the axial loading induced on both ends of the pipeline via the generalized nonlinear springs, result in an axial compression straining of the pipeline. This axial response of the pipeline is evaluated for an increasing level of relative axial ground displacement, δ_u, through a modified Riks solution algorithm. The main outcome of this analysis is a curve that describes the relation between an increasing relative axial ground displacement, δ_u, and the corresponding maximum compressive axial strain of the critical middle section of the pipeline, i.e. around the geotechnical discontinuity (see Step 3 in Fig. 3). It is noted that the analysis focuses on the axial ground displacements, which constitute the dominant loading mechanism for buried pipelines under seismic wave propagation, while it disregards the vertical ground displacements. Since the response of the pipeline is computed for an increasing level of relative axial ground displacement, δ_u, the outcome of one 3D SPI analysis may be used to evaluate the axial straining of the pipe under a variety of selected ground axial relative displacements, δ_{ue}, caused by diverse seismic motions. This may be possible with the utilization of 'mean' equivalent soil properties for the backfill soil, the latter corresponding to the strain-range that is anticipated for the selected ground seismic motions.

2.2.2 Step 2: Soil response analyses

In a second step, the seismic response of the selected soil sites is evaluated via 1D nonlinear soil response analyses, which are carried out separately for each subdeposit of the adopted pairs, employing DEEPSOIL [51]. Numerical models of the selected subdeposits, presented in *Section 2.1*, are initially developed, accounting also for the properties of the surficial ground layers (i.e. backfills) and the elastic bedrock. The models are then employed in a series of nonlinear time history analyses, using an ensemble of seismic records (see *Section 2.4*). The hysteretic nonlinear response of the soil during ground shaking is considered by means *G-γ-D* curves, which are properly selected for the examined deposits, following [41]. An additional viscous damping of 1 % is also introduced in the form of the frequency-dependent Rayleigh type [52], in order to avoid the potential amplification of higher frequencies of the ground that may result in unrealistic oscillations of the acceleration time histories in low ground strains. The Rayleigh coefficients are properly selected for a frequency interval range, characterizing the 'dominant frequencies' of each soil column. Through the soil response analyses, time histories of the horizontal deformations of the soil columns are calculated at the burial depths of the pipelines, which are then employed to compute maximum differential ground deformation patterns δ_{ue} for the selected pairs of adjusted subdeposits (see *Section 2.1*). Additionally, time histories of the horizontal acceleration, velocity and deformation are computed at the ground surface, in order to evaluate a variety of seismic *IMs* that are examined in the framework of this study.

### 2.2.3 Step 3: Combination of 3D SPI with 1D soil response analyses

The critical relative axial ground deformation patterns, δ_{ue} , which are defined based on the results of the 1D soil response analyses are finally correlated with the predicted straining of the

pipeline, using the δ_u - maximum compressive axial strain, ε, relations computed through the 3D SPI analyses.

Summarizing, the applying analytical framework accounts for critical parameters affecting the seismic response of buried steel pipelines. Additionally, the pseudo-static simulation of the seismically-induced transient ground deformations is computationally more efficient compared to an analysis conducted in a full-dynamic fashion.

Inevitably, the proposed analysis framework has some limitations. The inertial SPI effects, as well as effects of the evolution of stresses and deformations due to temperature changes on the pipeline response are not considered in the present study. Moreover, phenomena related to fatigue and steel strength and stiffness degradation due to cyclic loading, are neglected. The effect of soil nonlinearity during ground shaking, on the stiffness of the backfill and therefore on the confinement level of the pipeline, is considered in an approximate manner through the introduction of equivalent soil properties (i.e. strain-depended degraded stiffness) on the backfill. Additionally, the 1D soil response analyses cannot capture the potential 2D wave phenomena near the geotechnical discontinuity [53]. However, 1D nonlinear soil response analyses offer computational efficiency compared to 2D or 3D analyses and may be used as a first approximation for the evaluation of the seismic response of the ground and pipelines at shallow depths [53]. The computational efficiency of 1D soil response analyses allows for an extended and thorough parametric analysis, such as the one presented herein.

2.2.4 Verification of the 3D SPI model

As stated already, the length of the adopted 3D trench soil-pipe models was selected by examining various lengths and comparing the axial stresses and strains, computed at the middle critical section of the pipeline, with relevant predictions of equivalent 'infinitely' long 3D continuum models of the examined soil-pipe configurations, the latter subjected to the same axial ground deformation pattern. An example is provided in this section, referring to the $D = 914.4$ mm pipeline, embedded in a burial depth $h = 1.0$ m. The procedure followed to evaluate the nonlinear springs for the end-sides of the pipeline model in Fig. 3a, is initially presented in Fig. 6. More specifically, Fig. 6a illustrates the numerical model used to simulate the axial pull-out of the pipeline from the surrounding ground. The pull-out analyses were performed assuming a length for the model equal to 20 m and examining both adopted trench backfills, i.e. TA and TB (Table 5). The analyses yielded the shear stress-displacement relations presented in Fig. 6b. These relations were then used to define the maximum shear resistance τ_{max} and the shear stiffness k_s of the backfill soil-pipe interface, which were then employed in the definition of the nonlinear springs, following Eq (1). The computed force-displacement relations of the nonlinear springs for the present example are presented in Fig 6c. A higher friction coefficient for the backfill-pipe interface leads to 'stiffer' springs for the end-sides of the pipeline.
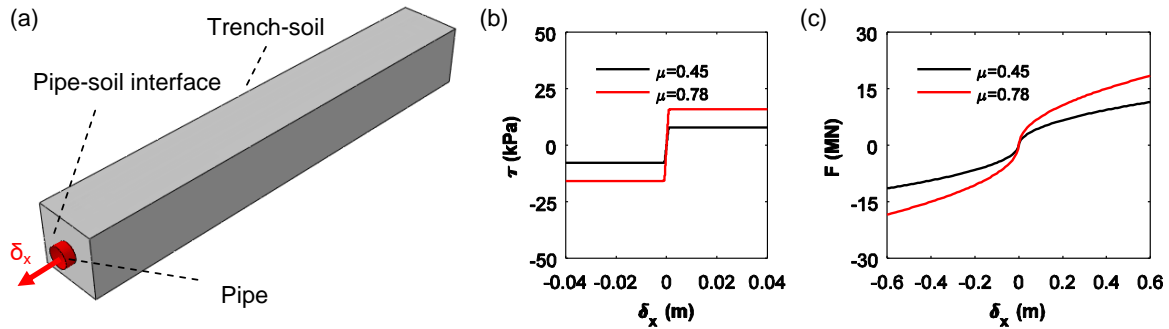
Fig. 6 (a) Numerical simulation of an axial pull-out test of a $D = 914.4$ mm pipeline, embedded at burial depth $h = 1.0$ m, (b) interface shear stress–displacement relationship estimated for the examined system when the pipeline is embedded in trench TA ($\mu = 0.45$) or in trench TB ($\mu = 0.78$), (c) force-displacement relations of the nonlinear springs, estimated as per Eq.1, when the examined pipeline is embedded in trench TA ($\mu = 0.45$) or in trench TB ($\mu = 0.78$).

The nonlinear springs were introduced at the end-sides of the examined pipeline and the numerical model was subjected gradually to a relative axial ground deformation up to $\delta_u = 20$ cm, as per Fig. 3a. The analyses were carried out for a 'perfect' pipeline (i.e. w/t=0), as well as for an equivalent pipeline with an initial geometric imperfection at the middle section (i.e. w/t=0.1). In both cases the pipeline was pressurized at an internal pressure $p = 8$ MPa. Fig. 7 compares representative numerical results of the pipelines responses computed by the proposed 3D SPI model, with relevant numerical predictions of extended 3D trench-pipe models of the examined pipelines (i.e. models with lengths equal to 500 times and 1000 times the diameter of the pipeline without springs at pipe edges). In particular, the axial stress (normalized over the yield Mises stress) and the axial strain computed along the ditch axis of the examined pipelines at the end of the analysis, i.e. after local buckling occurred, are compared. The extended models yield in almost identical results; therefore, it may be assumed that they may provide the response of an 'infinitely' long trench-pipeline model and can be used for verification purposes of the reduced length 3D hybrid model. The reduced length model provides similar results with the extended length models in terms of stresses and strains for both the perfect and imperfect pipelines, irrespectively of the adopted trench backfill properties. Evidently the computational cost of the reduced length model is highly reduced compared to the one of the extended models. It is worth noticing the significant effects of geometric imperfections of the walls of the pipeline, as well of the backfill properties and backfill-pipe interface frictional characteristics, on the axial response of the pipeline. Clearly, a much higher axial response is reported for the imperfect pipeline, embedded in trench TB (i.e. case of very-well compacted backfill soil with higher soil-pipe interface friction coefficient). The critical effects of pipeline wall imperfections or backfill compaction level on the axial response of buried steel pipelines are further examined in [47-48].
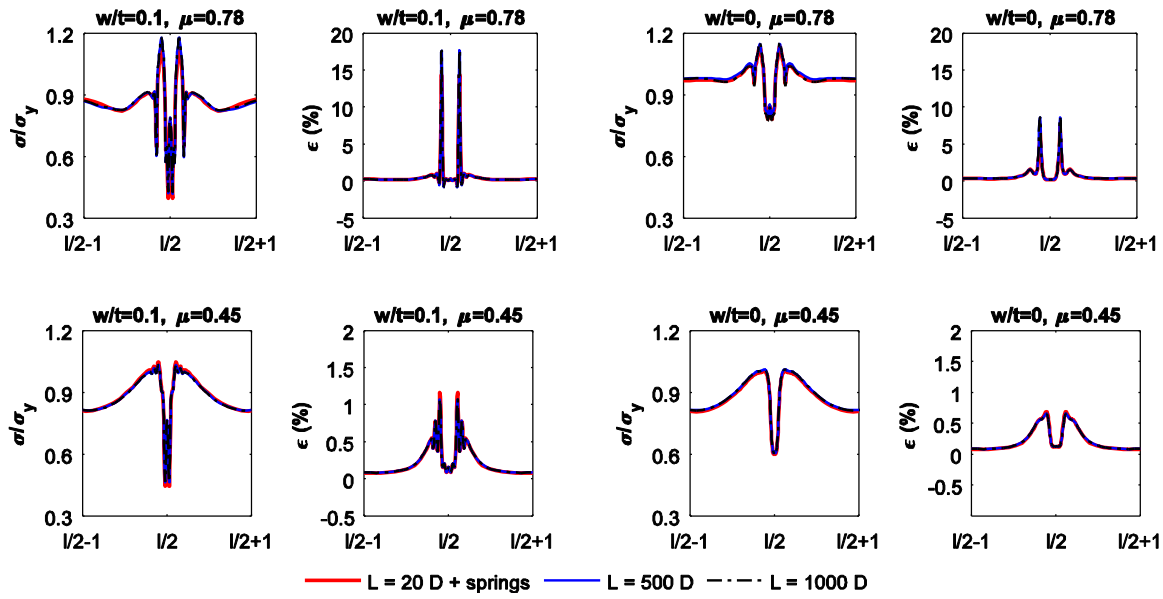
**Fig. 7** Comparisons of axial stresses (normalized over yield Mises stresses) and axial strains computed along the ditch axis of a D = 914.4 mm perfect (i.e. w/t=0) and imperfect (i.e. w/t=0.1) pipeline, embedded in trench TA (μ = 0.45) or TB (μ = 0.78) at a burial depth h = 1.0 m, by the 3D SPI model with the nonlinear springs at end-sides, (i.e. L = 20 D) and extended 3D SPI models (L = 500 D and L = 1000 D), the latter simulating the 'infinitely' long soil-pipeline configuration.

2.3 Seismic ground motions

An ensemble of 40 real ground motions, recorded on rock outcrop or very stiff soil (soil classes A and B according to Eurocode 8) [40] were selected in this study. The adopted records (Table 6), which were retrieved from the SHARE database [53], represent ground motions from earthquakes with moment magnitudes M_w, varying between 5 and 7.62, recoded at epicentral distances, R, between 3.4 and 71.4 km [36]. The shear wave velocity of first 30 m depth, $V_{s,30}$, of the recordings locations, ranges between 650 m/s and 2020 m/s. The peak ground acceleration PGA of the selected records varies between 0.065 g to 0.91 g. The peak ground velocity PGV ranges between 0.031 m/s to 0.785 m/s, while the Arias Intensity I_a, ranges from 0.015 m/s and 10.97 m/s. Scatter plots of the M_w-ln(R), PGA-PGV and PGA-I_a relations for the selected records are provided in Fig. 8. It is noted that no existing selection techniques that employ spectra for the selection of ground motions [e.g. as in 55-58] were used herein. This was done on the ground that the response of the extended buried pipelines is highly distinct compared to that of above ground structures (e.g. [59-60]), for which the 'target' spectra are actually defined. The selection is further strengthened by the fact that buried pipelines do not have an individual period of vibration, to which a spectrum could be conditioned.

Table 6. Selected ground motion records.

Date	Earthquake	Country	Station Name	Mw	R (km)	Preferred FS
25/07/2003	N Miyagi Prefecture	Japan	Oshika	6.1	32.00	Reverse
23/10/2004	Mid Niigata Prefecture	Japan	Tsunan	6.6	36	Reverse
12/06/2005	Anza	USA	Pinyon Flat Observatory	5.2	11.50	Strike-Slip
22/12/2003	San Simeon	USA	Ca: San Luis Obispo; Rec Center	6.4	61.5	Reverse
16/09/1978	Tabas	Iran	Tabas	7.35	57	Oblique
10/06/1987	Kalamata (Aftershock)	Greece	Kyparrisia-Agriculture Bank	5.36	17.00	Oblique
13/05/1995	Kozani	Greece	Kozani	6.61	17	Normal
07/09/1999	Ano Liosia	Greece	Athens 4 (Kipseli District)	6.04	17.00	Normal
15/04/1979	Montenegro	Serbia	Hercegnovi Novi-O.S.D.	6.9	65	Thrust
25/10/1984	Kremidia (Aftershock)	Greece	Pelekanada-Town Hall	5	16	
17/05/1995	Kozani (Aftershock)	Greece	Chromio-Community Building	5.3	16.00	Normal
13/10/1997	Kalamata	Greece	Koroni-Town Hall (Library)	6.4	48	Thrust
06/05/1976	Friuli	Italy	Tolmezzo-Diga Ambiesta	6.4	21.70	Reverse
15/09/1976	Friuli (Aftershock)	Italy	Tarcento	5.9	8.50	Reverse
23/11/1980	Irpinia	Italy	Bisaccia	6.9	28.30	Normal
14/10/1997	Umbria Marche (Aftershock)	Italy	Norcia	5.6	20.00	Normal
09/09/1998	App. Lucano	Italy	Lauria Galdo	5.6	6.60	Normal
06/04/2009	L Aquila Mainshock	Italy	L Aquila - V. Aterno - Colle Grilli	6.3	4.40	Normal
09/02/1971	San Fernando	USA	Lake Hughes #12	6.61	20.04	Reverse
28/11/1974	Hollister-03	USA	Gilroy Array #1	5.14	11.08	Strike-Slip
06/08/1979	Coyote Lake	USA	Gilroy Array #6	5.74	4.37	Strike-Slip
02/05/1983	Coalinga-01	USA	Slack Canyon	6.36	33.52	Reverse
24/04/1984	Morgan Hill	USA	Gilroy Array #6	6.19	36.34	Strike-Slip
23/12/1985	Nahanni, Canada	Greece	Site 1	6.76	6.8	Reverse
14/11/1986	Taiwan Smart1(45)	Taiwan	Smart1 E02	7.3	71.35	Reverse
07/02/1987	Baja California	USA	Cerro Prieto	5.5	3.69	Strike-Slip
18/10/1989	Loma Prieta	USA	Gilroy Array #6	6.93	35.47	Reverse-Oblique
18/10/1989	Loma Prieta	USA	Ucsc Lick Observatory	6.93	16.34	Reverse-Oblique
25/04/1992	Cape Mendocino	USA	Petrolia	7.01	4.51	Reverse
28/06/1992	Landers	USA	Lucerne	7.28	44.02	Strike-Slip
17/01/1994	Northridge-01	USA	La - Griffith Park Observatory	6.69	25.42	Reverse
17/01/1994	Northridge-01	USA	Pacoima Dam (Downstr)	6.69	20.36	Reverse
16/01/1995	Kobe, Japan	Japan	Nishi-Akashi	6.9	8.7	Strike-Slip
20/09/1999	Chi-Chi, Taiwan	Taiwan	Tcu071	7.62	15.42	Reverse-Oblique
28/06/1991	Sierra Madre	USA	Mt Wilson - Cit Seis Sta	5.61	6.46	Reverse
16//10/1999	Hector Mine	USA	Hector	7.13	26.53	Strike-Slip
20/09/1999	Chi-Chi, Taiwan-03	Taiwan	Tcu129	6.2	18.5	Reverse
17/08/1999	Izmit	Turkey	Gebze-Tubitak Marmara	7.6	42.77	Strike-Slip
17/08/1999	Izmit	Turkey	Izmit-Meteoroloji Istasyonu	7.6	3.40	Strike-Slip
12/11/1999	Duzce 1	Turkey	Ldeo Station No. C1058 Bv	7.1	15.60	Strike-Slip
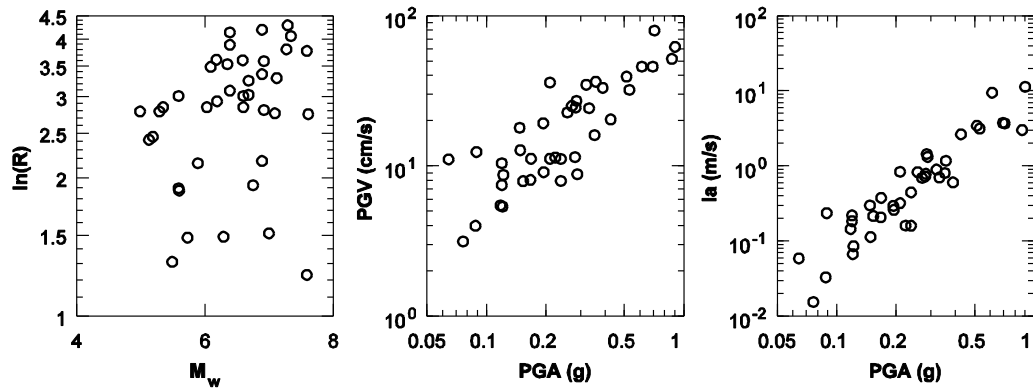
Fig. 8 Distribution of main parameters of selected ground motion records.

3. Selection of seismic intensity measures

A variety of seismic *IMs* has been employed in the existing literature to describe seismic intensity in empirical fragility functions for the structural assessment of buried pipelines [61-62], including the Modified Mercalli Intensity *MMI* [63-67], the peak ground acceleration *PGA* [68-70], the peak ground velocity *PGV* [6-7,38,67,71-79], the peak ground strain (ε_g) [11,77,79], as well as PGV^2/PGA [80]. The efficiency of Arias intensity I_a, spectral acceleration *SA* and spectral intensity *SI*, in predicting the damage of buried pipelines under transient ground deformations was also examined in previous studies [67, 81]. The limited available analytical fragility curves for buried steel NG pipelines make use of *PGA* and *PGV* as seismic *IMs* [82-83]. From the above seismic *IMs*, *PGV* and ε_g, are those that are directly related to the main loading condition, which is responsible for the induced damage on buried pipelines caused by seismically-induced transient ground deformations.

Shakib and Jahangiri [37] examined the efficiency and sufficiency of various seismic *IMs* for buried steel NG pipelines, employing a numerical parametric study on selected pipe-soil configurations. In addition to the above seismic *IMs* (*e.g. PGA, PGV, PGV^2/PGA, I$_a$*), a set of other measures was also examined, including the peak ground displacement, *PGD*, the root mean square acceleration, velocity and displacement, RMS_a, RMS_v, RMS_d, PGD^2/RMS_d, the cumulative absolute velocity, *CAV*, the sustained maximum acceleration and velocity, *SMA*, *SMV* and a series of spectral *IMs*. The researchers proposed spectral seismic *IMs* as optimal ones for some of the examined pipe-soil configurations. However, to the authors' view, the use of spectral seismic *IMs* for embedded structures, such as buried pipelines, might be highly debatable, when considering the kinematic loading, which is imposed by the surrounding ground on the embedded pipeline under ground shaking and is prevailing over the pipeline's inertial response [5, 59-60]. Actually, buried structures (including pipelines) exhibit a highly distinct seismic response compared to that of single degree of freedom oscillators (SDOF), for which the response spectra and the relevant spectral seismic *IMs* are defined. This perspective comes in line with the poor correlations between spectral seismic *IMs*, i.e. spectral acceleration and spectrum intensity, and observed damage on water-supply and steel NG pipelines during past earthquakes [67, 81]. Based on the above observations, no spectral seismic *IMs* were examined herein.

Table 7 summarizes the tested seismic *IMs*. The selected *IMs* have been widely used in previous studies, e.g. for the development of empirical fragility functions or analytical fragility relations, while most of them may be evaluated easily. Hazard maps and hazard curves are readily available in terms of *PGA* or *PGV*, while other seismic *IMs*, such as Arias intensity I_a require more effort to be evaluated. Along these lines, *PGA* or *PGV* might be more desirable, particularly in the framework of a rapid post-seismic assessment of an extended NG network and management of the post-seismic risk [84]. The peak longitudinal ground strain ε_g was not examined herein, due to the nature of the soil response analyses that were carried out within this study (i.e. 1D soil response analyses). Despite of the direct correlation of longitudinal ground strain with pipeline axial response, its rigorous computation or even its evaluation in a simplified fashion via *PGV* and wave propagation velocity *C* of the site (i.e. $\varepsilon_g = PGV/C$) may be cumbersome [61], particularly in the presence of strong soil heterogeneities along the pipeline axis, like in the cases examined herein. The selected seismic *IMs* refer to either outcrop conditions or ground surface conditions. For the latter cases, two computation approaches were examined since multiple values of the seismic *IMs* are available near the geotechnical discontinuity of the examined soil deposits, i.e. those computed at the ground surface above subdeposit 1 and those computed at the ground surface above subdeposit 2 (Fig. 1). In particular, the seismic *IMs* at the ground surface refer to either the maximum value of the peak values computed at the surface adjacent subdeposits, or to the mean value of the peak values predicted at the adjacent subdeposits (see Table 7).

Table 7 Examined Intensity Measures.

Location	Intensity measure
Outcrop	Peak ground acceleration $\quad PGA_r = \max\lvert a_r(t) \rvert$
Outcrop	Peak ground velocity $\quad PGV_r = \max\lvert v_r(t) \rvert$
Outcrop	Peak ground velocity $\quad PGD_r = \max\lvert d_r(t) \rvert$
Outcrop	Arias intensity $\quad Ia_r = \dfrac{\pi}{2g}\displaystyle\int_0^\infty \left[a_r(t) \right]^2 dt$
Ground surface	Peak ground acceleration $\quad PGA_1 = \max\left\{ \max\lvert a_{soil,1}(t) \rvert, \max\lvert a_{soil,2}(t) \rvert \right\}$
Ground surface	Peak ground acceleration $\quad PGA_2 = avg\left\{ \max\lvert a_{soil,1}(t) \rvert, \max\lvert a_{soil,2}(t) \rvert \right\}$
Ground surface	Peak ground velocity $\quad PGV_1 = \max\left\{ \max\lvert v_{soil,1}(t) \rvert, \max\lvert v_{soil,2}(t) \rvert \right\}$
Ground surface	Peak ground acceleration $\quad PGV_2 = avg\left\{ \max\lvert v_{soil,1}(t) \rvert, \max\lvert v_{soil,2}(t) \rvert \right\}$
Ground surface	Peak ground acceleration $\quad PGD_1 = \max\left\{ \max\lvert d_{soil,1}(t) \rvert, \max\lvert d_{soil,2}(t) \rvert \right\}$
Ground surface	Peak ground acceleration $\quad PGD_2 = avg\left\{ \max\lvert d_{soil,1}(t) \rvert, \max\lvert d_{soil,2}(t) \rvert \right\}$
Ground surface	$PGV^2/PGA_1 = \max\left\{ \max PGV^2/PGA_{soil,1}, \max PGV^2/PGA_{soil,2} \right\}$
Ground surface	$PGV^2/PGA_2 = avg\left\{ \max PGV^2/PGA_{soil,1}, \max PGV^2/PGA_{soil,2} \right\}$

4. Intensity measure testing

4.1 Efficiency of tested seismic *IMs*

To test the efficiency of the selected seismic *IMs*, regression analyses of the *EDP*, i.e. the numerically predicted maximum compression strain ε of the examined pipelines at the critical middle section, relative to each seismic *IM* were carried out. A power model was initially employed to describe the relationship between the pipe compression strain ε and the tested seismic *IM* [85]:

$$EDP = a \times \left(IM \right)^{b} \qquad (9)$$

where a and b are coefficients defined by the regression analysis. The above relation may be rearranged in a linear regression analysis of the natural logarithm of the *EPD* relative to the natural logarithm of the tested seismic *IM*, as follows:

$$ln\left(EPD \right) = b \times ln\left(IM \right) + a + \varepsilon_{res} \times \sigma \qquad (10)$$

where ε_{res} is the standard normal variant with zero mean and unit standard deviation and σ is a dispersion parameter, describing the conditional standard deviation of the regression. The latter is defined in natural logarithm units and constitutes a metric of the *efficiency* of the tested seismic *IM* with respect to the *EPD*. Lower σ values mean reduced dispersion around the estimated median of the results, which in other words means a more efficient seismic *IM*. A representative example of a regression analysis of the *EPD* versus PGV_1 is presented in Fig. 9, referring to a $D = 914.4$ mm 'perfect' pipeline pressurized at $p = 8$ MPa and embedded in trench TA. The examined soil-pipe system is assumed to be located over the examined pairs of soil subdeposits (see *Section* 2.1), while the ground depth H is equal to 60 m.
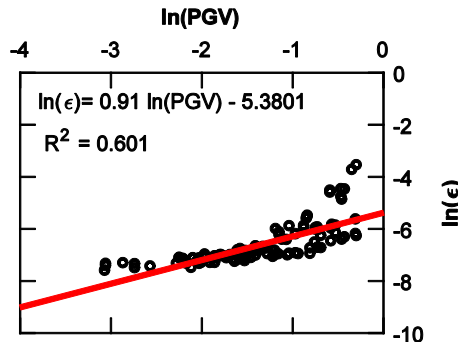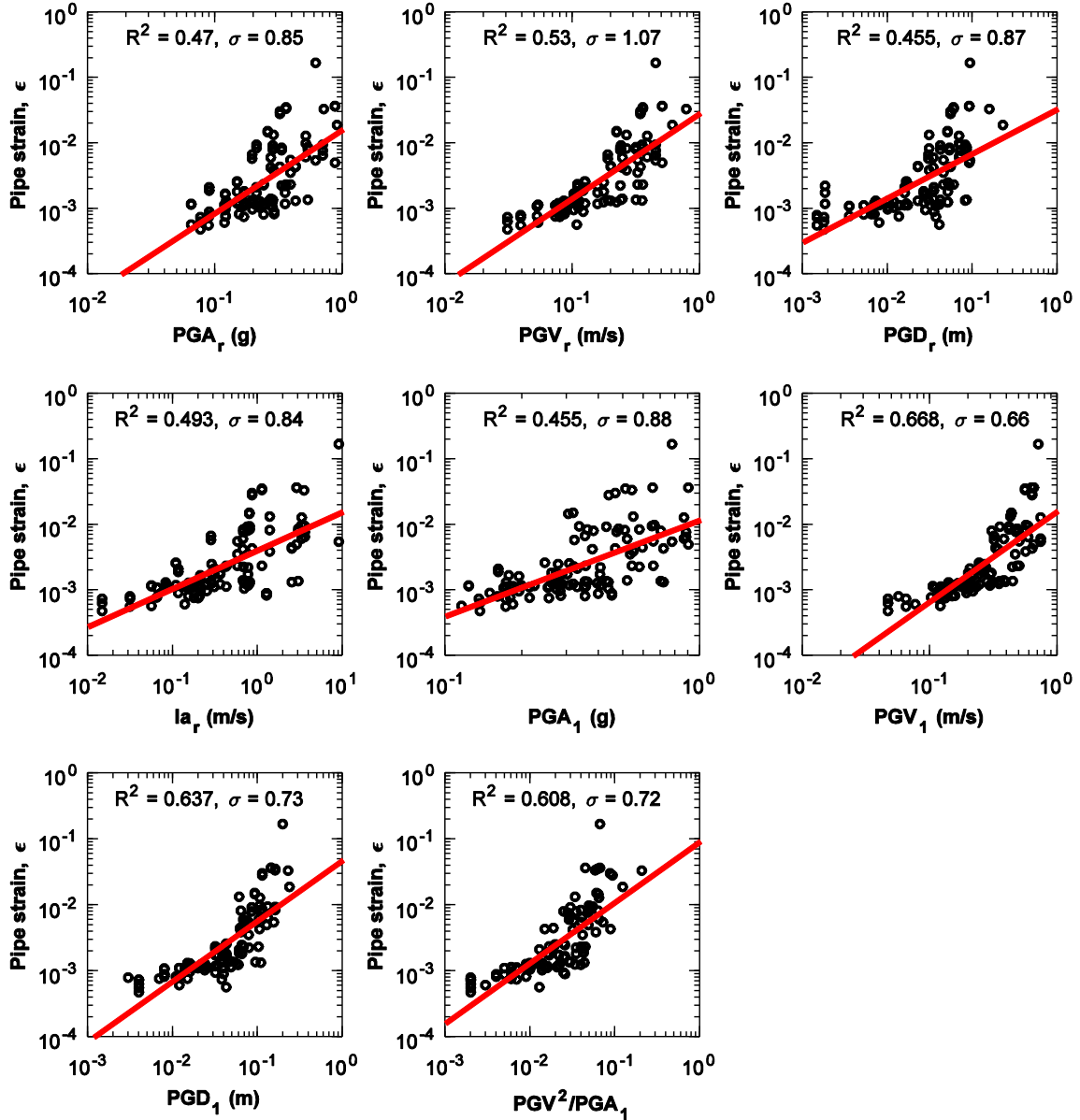

Fig. 9 Regression analysis of the natural logarithm of the maximum compression strain ε of the pipeline (computed at the critical middle section) relative to the natural logarithm of the PGV_1 at ground surface (results for a $D = 914.4$ mm 'perfect' pipeline embedded in trench TA in soil deposits with $H = 60$ m).

Fig. 10 summarizes representative regression analyses of the maximum pipeline compression strain, ε, relative to various seismic *IMs* tested herein. The regressions refer to a X60 $D = 914.4$ mm 'perfect' pipeline, pressurized at $p = 8$ MPa and embedded in trench TA in soil deposits with depth $H = 30$ m. The seismic *IMs*, referring to ground surface conditions, are computed as the maximum value of the peak values of the measures computed at the adjacent subdeposits, i.e. *IMs$_1$*, according to Table 7. It is noted that the regressions were conducted in the log-log space; however, both the compression strains and the seismic *IMs* are displayed in their actual units in Fig. 10. Similar regressions are provided in Fig. 11, referring to the same pipeline,

1   embedded this time in trench TB in soil deposits with depth $H = 30$ m. In both cases, the lowest
2   standard deviations σ are reported for the peak ground velocity at the ground surface, PGV_1,
3   (i.e. $\sigma = 0.52$ and 0.66 when the pipeline is embedded in trench TA and TB, respectively),
4   implying that this seismic IM is the most efficient one, compared to other tested measures. This
5   observation is in line with the theoretically expected superiority of PGV over the other seismic
6   IMs tested herein. As stated above, PGV is related directly with the ground strains that are
7   imposed along buried pipelines during ground shaking and constitute the main loading
8   mechanism of this infrastructure under this loading condition. A reduced standard deviation
9   (compared to the other seismic IMs) is also reported for PGV^2/PGA_1, i.e. $\sigma = 0.55$ and 0.72 for
10 pipeline in trench TA and TB, respectively). The most inefficient seismic IMs for the examined
11 soil-pipe configurations are found to be PGA_1 ($\sigma = 0.64$), when the pipeline is embedded in
12 trench TA and PGV_r ($\sigma = 1.07$), when the pipeline is embedded in trench TB. Interestingly,
13 higher standard deviations σ are computed when the pipeline is embedded in the trench TB. It
14 is recalled that in this case, a denser backfill material and a higher friction coefficient for the
15 backfill-pipe interface are considered. For a given ground deformation pattern, the above
16 conditions will lead to higher shear stresses along the perimeter of the pipeline, compared to
17 the shear stresses developed along the pipeline, when this is embedded in a looser backfill with
18 reduced friction at soil-pipeline interface (i.e. trench TA). These higher shear stresses along the
19 perimeter of the pipeline will result in its higher axial loading, thus increasing the potential of
20 its yielding or buckling failure. The higher nonlinear axial response of the pipeline increases
21 the scatter of the numerically predicted pipe strain ε for a given value of the seismic IMs,
22 finally leading to higher σ values, as observed in the regression analyses of Fig. 11.
23
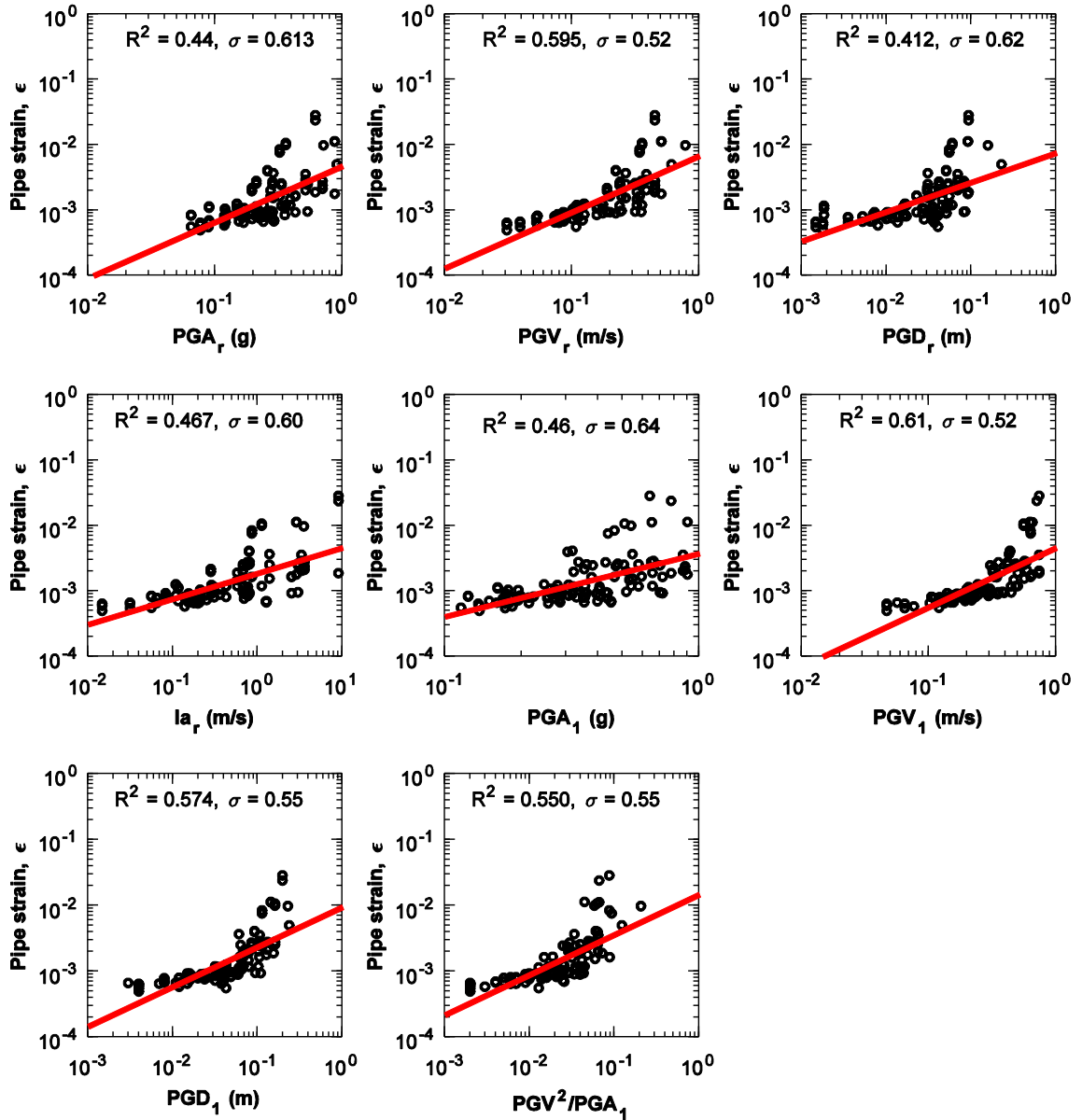
Fig. 10 Regression analyses for testing the efficiency of various seismic *IMs,* referring to outcrop conditions or ground surface conditions (results for a X60 *D* = 914.4 mm 'perfect' pipeline, pressurized at *p* = 8 MPa and embedded in trench TA in soil deposits of depth *H* = 30 m; *ε*: compression axial strain computed at the critical middle section of the pipeline).

1
2 **Fig. 11** Regression analyses for testing the efficiency of various seismic *IMs,* referring to outcrop
3 conditions or ground surface conditions (results for a X60 D = 914.4 mm 'perfect' pipeline, pressurized
4 at p = 8 MPa and embedded in trench TB in soil deposits of depth H = 30 m; ε: compression axial strain
5 computed at the critical middle section of the pipeline).
6
7 Figs. 12-14 compare the standard deviations σ computed for all tested seismic *IMs* in all
8 examined cases. Through the comparisons, the effects of salient parameters controlling the
9 axial response of the buried steel pipelines, on the computed σ values are reported.
10 Fig. 12a summarizes standard deviations σ computed for D = 914.4 mm pipelines, embedded
11 at a burial depth h = 1.0 in trench TA in diverse soil deposits with depth H = 30 m. The
12 comparisons highlight the effects of steel grade and internal pressure of the pipeline, as well as
13 of imperfections of the walls of the pipeline on the computed standard deviations σ. In this
14 context, the standard deviations are plotted for X60, X65, X70 'perfect' (i.e. w/t = 0) or
15 imperfect (i.e. w/t = 0.1) pipelines, pressurized at various levels of internal pressure (i.e. p = 0,
16 4 or 8 MPa). The standard deviations computed for all tested seismic *IMs* are generally

increasing with decreasing steel grade, i.e. higher σ values are reported for X60-grade pipelines compared to those calculated for X65- or X70-grade pipelines. Similarly, higher standard deviations σ are reported for the imperfect pipelines (i.e. $w/t = 0.1$) compared to the equivalent 'perfect' ones (i.e. $w/t = 0$). Moreover, in case of imperfect pipelines (i.e. $w/t = 0.1$) it is found that the increase of the internal pressure of the pipeline leads to an increase of the standard deviations σ. The latter observation is found to be invalid for perfect pipelines (i.e. $w/t = 0$), as higher standard deviations σ are reported for non-pressurized pipelines ($p = 0$ MPa) compared to those calculated for pipeline pressurized at $p = 4$ MPa. The above observations should be attributed to the effect of the examined parameters (i.e. pressure level, pipeline wall imperfections and steel grade) on the axial response of the pipeline under seismically-induced ground deformations. For a given soil-pipeline configuration subjected to a given seismic ground deformation pattern, the reduction of the steel grade of the pipeline will lead to an increased nonlinear axial response of the pipeline, which will finally result in the higher standard deviations σ, reported for lower steel grade pipelines in Fig. 12a. The existence of wall imperfections on the pipeline is again expected to lead in a higher nonlinear axial response of the pipeline, compared to that of an equivalent 'perfect' pipeline-soil system subjected to the same ground deformation pattern [44, 47-48]. This may explain the higher σ values reported for imperfect pipelines (i.e. $w/t = 0.1$), compared to those reported for equivalent 'perfect' pipelines (i.e. $w/t = 0$).

Previous studies [44-48] have demonstrated that pressurization of steel pipelines leads to initial circumferential tensile stresses, which interact with the axial straining of the pipeline, caused by the seismically-induced ground deformation. In particular, the increase of the internal pressure level of the pipeline tends to lower the axial load-displacement path, leading faster to yielding or instability phenomena. In other words, for a given soil-pipeline configuration subjected to a given seismic ground deformation pattern, the increasing pressurization of the pipeline is expected to lead to an increasing nonlinear axial response of the pipeline under the induced ground deformation, which subsequently will lead to a higher scatter of the pipeline strain ε against the tested seismic *IMs*. This is confirmed in Fig. 13a since higher σ values are computed for pipelines pressurized at $p = 8$ MPa, compared to those predicted for $p = 0$ or 4 MPa.

Regardless of the effects of the above parameters on the computed σ values, the lowest standard deviations are reported for PGV_1, followed by PGV_2 and PGV_r. PGV^2/PGA_1 and PGV^2/PGA_2 are also found to give relatively low σ values. On the contrary the highest standard deviations are reported for PGA_2 followed by PGA_1 and PGA_r. Ia_r and PGD_1, PGD_2 and PGD_r are found to be rather inefficient *IMs* as compared to the *PGV* metrics.
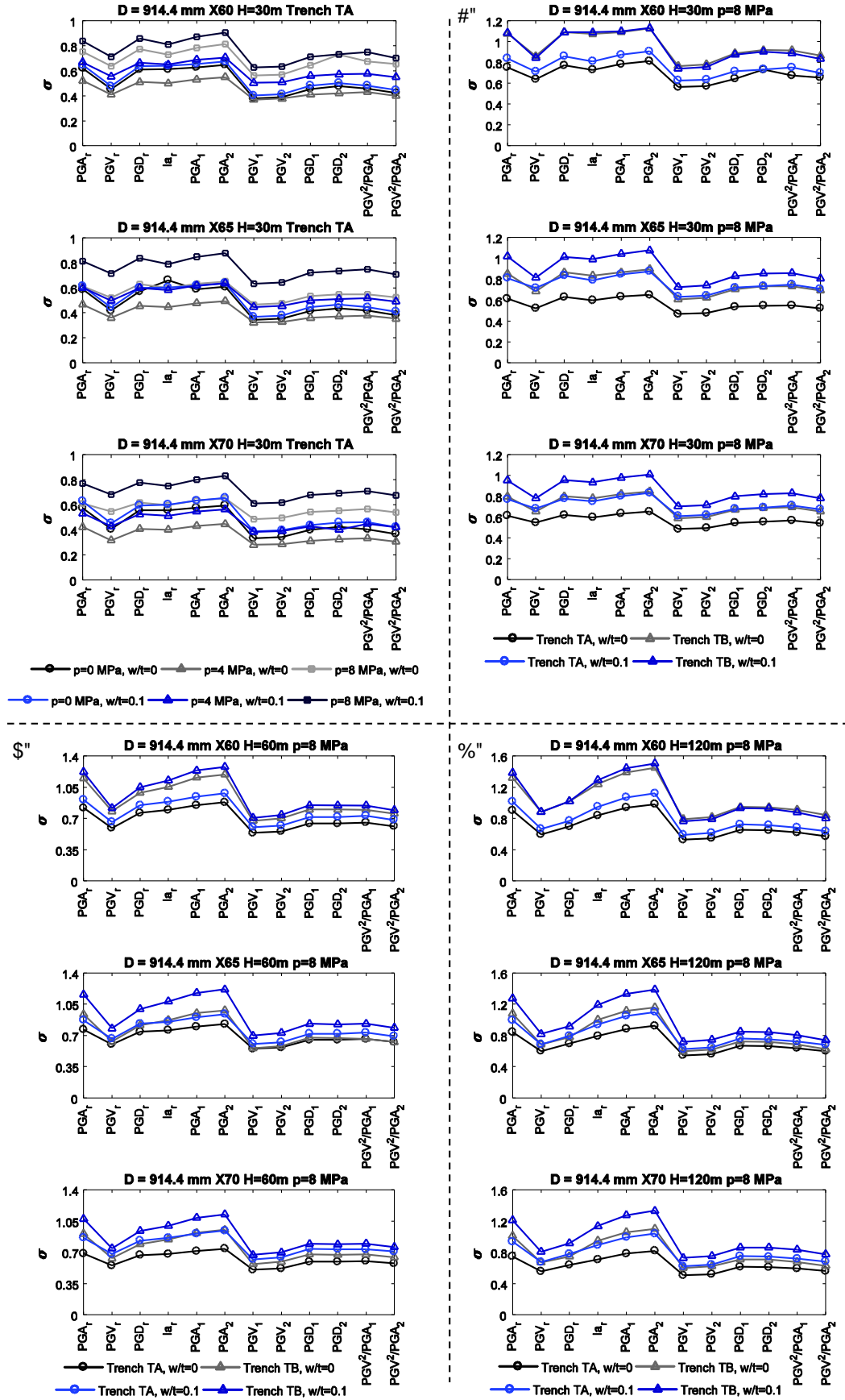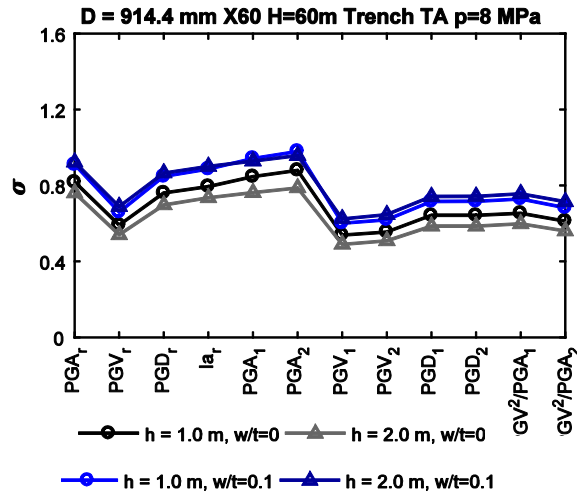
Fig. 12 Comparisons of standard deviations σ computed for D = 914.4 mm pipelines through regression analyses of the axial compression strain ε of pipelines relative to tested seismic *IMs*. (a) Effects of internal pressure p and pipeline wall imperfections (*w/t*) on σ values. (b) Effect of trench

1   backfill properties and soil-pipe interface characteristics on σ values. (c, d) Effect of soil deposit depth

2   H on σ values.

3

4   Fig. 12b elaborates on the effects of backfill properties and backfill-pipeline interface friction

5   characteristics on the standard deviations σ, estimated for all tested seismic *IMs*, by

6   comparing σ values computed for X60, X65 or X70 $D = 914.4$ mm pipelines, embedded at a

7   burial depth $h = 1.0$ in either trench TA or TB. The comparisons are provided for soil deposits

8   with depth $H = 30$ m and refer to both 'perfect' (i.e. $w/t = 0$) and imperfect pipelines (i.e. $w/t =$

9   0.1), pressurized at a pressure level $p = 8$ MPa. Higher σ values are clearly observed for the

10 cases where the pipelines are embedded in trench TB, where a higher compaction level of the

11 backfill and a higher backfill-pipe interface friction coefficient are considered. These

12 observations, which are related to the increased axial response of the pipelines when embedded

13 in trench TB, are in line with the observations made above (i.e. by comparing the regression

14 analyses in Figs. 10 and 11). Regardless of the trench properties and the soil-pipeline interface

15 characteristics, PGV_1 exhibits again the lowest standard deviations in all examined cases,

16 whereas the highest standard deviations are reported for PGA_2. Similar conclusions are drawn

17 when the examined pipelines (i.e. X60, X65 or X70 $D = 914.4$ mm 'perfect' or imperfect

18 pipelines) are embedded in soil deposits with higher depths, i.e. $H = 60$ m (i.e. Fig. 12c) or $H =$

19 120 m (i.e. Fig. 12d). In both cases PGV_1 exhibits the lowest standard deviations, whereas the

20 highest standard deviations are reported for PGA_2. It is worth noticing the increasing σ values

21 reported for all tested seismic *IMs* with increasing depth, H, of the soil deposits. The latter

22 observation should be attributed to the higher differential ground response of deeper adjacent

23 subdeposits, compared to that of shallower deposits under a given seismic excitation at

24 bedrock. The higher differential ground response of the adjacent subdeposits is expected to

25 induce a higher axial straining on the pipeline, thus increasing the potential of a more

26 'nonlinear' response of the pipeline, which results in the higher standard deviation values in the

27 relevant comparisons.

28 Fig. 13 examines the effect of burial depth of the pipeline on the standard deviations σ

29 estimated for all tested seismic *IMs*, by comparing the relevant σ values computed for X60 $D =$

30 914.4 mm pipelines embedded at depths $h = 1.0$ m or 2.0 m in trench TA in soil deposits with

31 depth $H = 60$ m. The relevant comparisons refer to both 'perfect' (i.e. $w/t = 0$) and 'imperfect'

32 (i.e. $w/t =0 .1$) pipelines, pressurized at a pressure level $p = 8$ MPa. Higher standard deviations

33 are computed in most cases for the shallow-embedded pipelines (i.e. for $h = 1.0$ m) compared

34 to the equivalent pipelines embedded at $h = 2.0$ m. This observation is due to the increased

35 ground response of the soil subdeposits towards ground surface, which yields in a higher

36 relative axial ground deformation along the pipeline axis, therefore triggering a higher

37 nonlinear axial response of shallower pipelines compared to the equivalent deeper 'equivalent'

38 pipelines. In line with the previous results, higher σ values are reported for all tested seismic

39 *IMs* in case of imperfect pipelines (i.e. $w/t = 0.1$). Irrespectively of the pipeline's burial depth,

40 PGV_1 exhibits the lowest σ values, while the highest values are reported for PGA_2 and PGA_1.

Fig. 13 Effect of burial depth, h, of the pipeline on standard deviations σ computed through regression analyses of the axial compression strain ε of pipeline, relative to tested seismic *IMs*. Results for X60 D = 914.4 mm pipelines embedded in trench TA in soil subdeposits with depth H = 60 m.

Fig. 14a summarizes the standard deviations σ computed for all tested seismic *IMs* in case of D = 406.4 mm pipelines. More specifically, the presented σ values refer to X60, X65 and X70 perfect (w/t =0) and imperfect (w/t=0.1) pipelines, pressurized at a pressure level p = 8 MPa and embedded in trench TA or TB in diverse soil deposits with depth H = 60 m. Similar to the previous results, higher standard deviations are computed for imperfect pipelines (w/t =0.1) embedded in trench TB. Additionally, higher σ values are reported for lower steel grade pipelines compared to those predicted for equivalent higher steel grade pipelines; however, the differences between the σ values computed for various steel grade pipelines are found reduced as compared to the D =914.4 mm pipelines. Similar observations and conclusions are made for D = 1219.2 mm pipelines examined in this study (Fig. 14b). Regardless of the geometrical properties of the examined pipelines, PGV_1, reveals the lowest standard deviations σ, for all examined cases.

Summarizing, the lowest standard deviations are reported for PGV_1 for all examined soil-pipe configurations. Hence, this seismic *IM* is considered the most efficient from the tested ones. On the contrary, *PGA*-based measures at top of ground surface (i.e. PGA_1, PGA_2) are found to be the most inefficient ones, as they exhibit the highest standard deviations for all examined configurations. The above observations are valid, irrespectively of the diameter and wall thickness of the pipeline. However, lower dispersion values are generally identified for the D = 1219.2 mm pipelines with the thicker walls (i.e. R/t = 31.9).
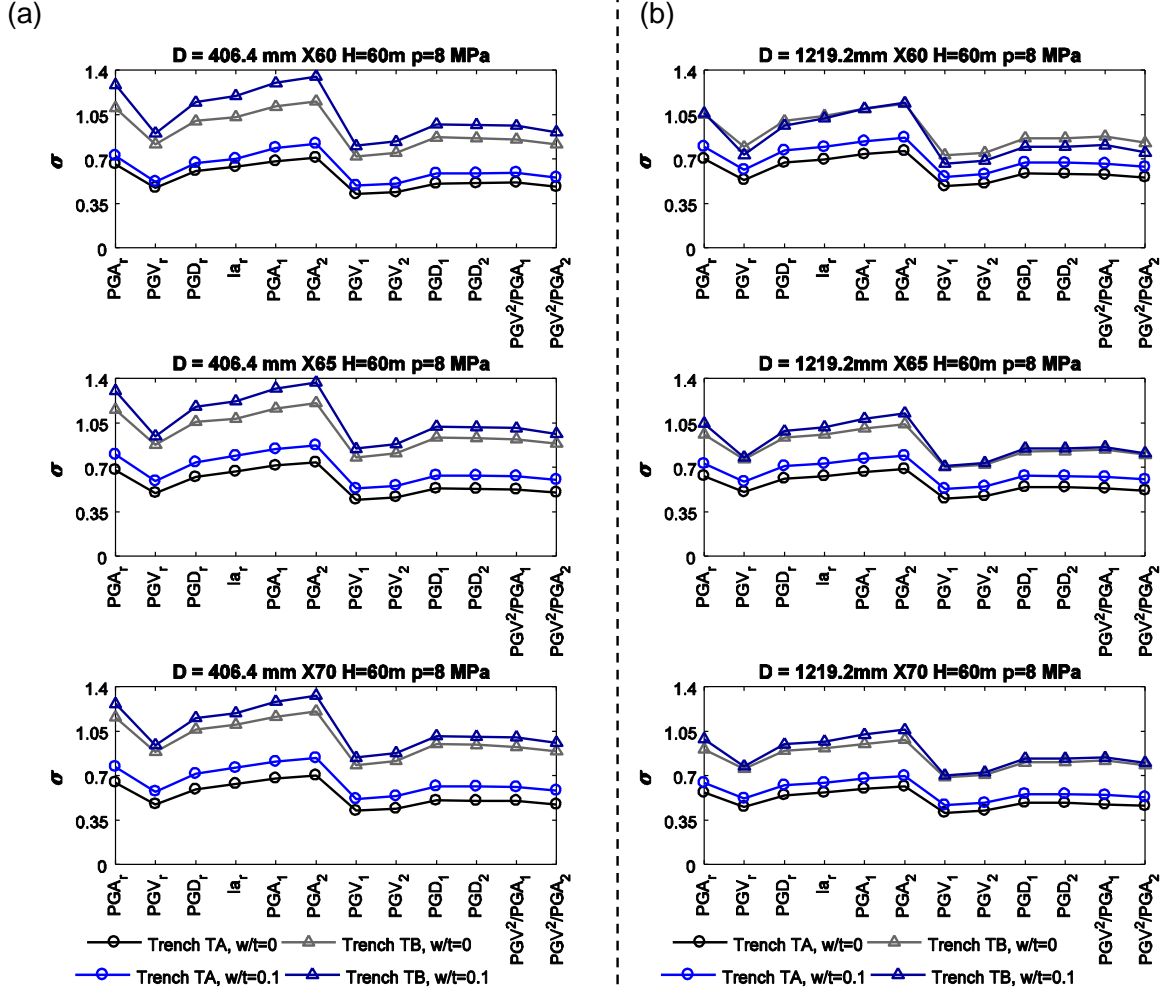
Fig. 14 Comparisons of standard deviations σ computed for D = 406.4mm (a) and D = 1219.2 mm (b) pipelines through regression analyses of the axial compression strain ε of pipelines relative to tested seismic *IMs*.

4.2 Sufficiency of tested seismic *IMs*

As stated above, a *sufficient* seismic *IM* is conditionally independent of the seismological characteristics, such as the magnitude (*M*) and the epicentral distance (*R*) [28]. To determine the sufficiency of the tested seismic *IMs*, regression analyses were performed on the residuals of the compression axial strain ε of the pipeline (referring at the middle critical section of the pipeline), relative to the magnitude and the epicentral distance of the selected seismic records (i.e. $\varepsilon_{res}|IM$). The residuals $\varepsilon_{res}|IM$ were defined as the differences between the numerically computed maximum pipeline axial strains (3D SPI results) and the strains computed by the regression fit line, the latter defined by the regression analysis on the maximum axial strain ε relative to the tested seismic *IM* (i.e. regression analysis conducted in the framework of identifying the efficiency of the tested *IM*, e.g. Fig. 9). The sufficiency was quantified by extracting the relevant *p*-values from the regressions of $\varepsilon_{res}|IM$ relative to the seismological characteristics of the selected ground motions, i.e. *M* and *R*. Fig. 15 illustrates examples of such regression analyses, referring to a X60 D = 914.4 mm 'perfect' pipeline embedded at a burial depth *h* =1.0 m in trench TA in soil deposits with depth *H* = 30 m. The analyses were

1 conducted for the selected ground motions to examine the sufficiency of PGV_1. Sufficient
2 seismic *IMs* generally lead to high *p-values*. A cut-off *p*-value of 0.05 was set here to
3 differentiate between sufficient and insufficient seismic *IMs* [28].
4
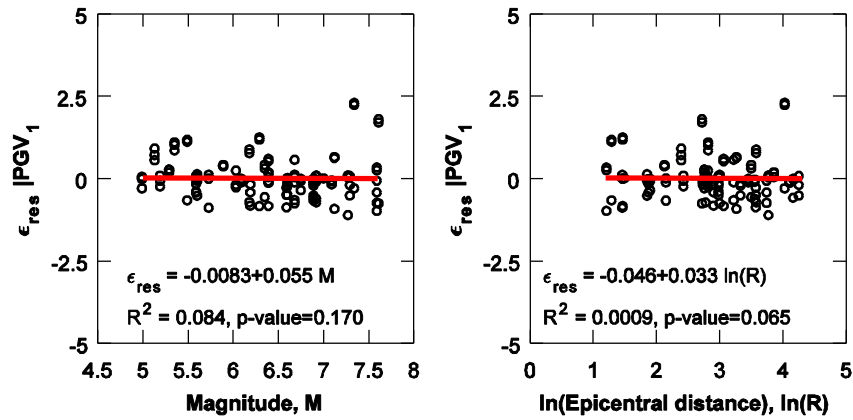
5
6 **Fig. 15** Representative regression analyses of $\varepsilon_{res}\big|IM$ relative to magnitudes (*M*) and epicentral
7 distances (ln(*R*)) of selected ground motions, aiming at evaluating the sufficiency of PGV_1. Results for a
8 X60 *D* = 914.4 mm 'perfect' pipeline, embedded in trench TA in soil deposits with depth *H* = 30 m and
9 pressurized at *p* = 8 MPa.
10

11 Figs. 16-18 summarize the *p-values* computed for all tested seismic *IMs* in all examined cases,
12 based on regression analyses of the residuals of the compression axial strain ε of the pipeline
13 ($\varepsilon_{res}\big|IM$) relative to the magnitude of the selected seismic records. In particular, Fig. 16a
14 summarizes *p-values* computed for *D* = 914.4 mm pipelines, embedded at a burial depth *h* =
15 1.0 in trench TA in diverse soil deposits with depth *H* = 30 m. The comparisons aim at
16 highlighting the effects of steel grade and internal pressure of the pipeline, as well as of
17 imperfections of the walls of the pipeline on the computed *p-values*. No clear trends can be
18 identified regarding the effects of pipeline internal pressure on the *p-values*. However, slightly
19 higher *p-values* (up to 5%) are computed for most of tested seismic *IMs* and examined
20 configurations, with decreasing internal pressure of the pipeline. The same trend, i.e. higher *p-*
21 *values*, is observed with increasing steel grade of the pipeline, while a slight decrease of *p-*
22 *values* is observed for imperfect pipelines (i.e. *w/t* =0.1) compared to 'perfect' equivalent ones
23 (i.e. *w/t* = 0). Irrespectively of the steel grade, internal pressure and shape of the walls of the
24 pipeline, it can be clearly seen that PGV_1 exhibits the highest *p-values* compared to the other
25 tested seismic *IMs*. Relatively high values are reported for the PGV_2 and PGV_r, while PGD_r,
26 IA_r, PGD_1, PGD_2, PGV^2/PGA_1 and PGV^2/PGA_1 are found to pass the threshold limit of 0.05 for
27 the *p-value*, in most of examined cases. On the contrary, the *p-values* computed for PGA_1,
28 PGA_2 and PGA_r are in most of examined cases lower than the threshold (i.e. 0.05), indicating
29 that these measures are insufficient *IMs* for the examined systems.
30 Fig. 16b-d aim at highlighting the effects of soil deposit depth, *H*, backfill properties and
31 backfill-pipeline interface friction characteristics on the computed *p-values*, the latter estimated
32 again via regression analyses of the residuals of the compression axial strain ε of the pipeline
33 ($\varepsilon_{res}\big|IM$) relative to the magnitudes of the selected seismic records. The results refer to X60,

1 X65 or X70 D = 914.4 mm 'perfect' (i.e. w/t = 0) and imperfect pipelines (i.e. w/t = 0.1)
2 pipelines, embedded at a burial depth h = 1.0 in either trench TA or TB in soil deposits of
3 depth H = 30 m (Fig. 16b), H = 60 m (Fig. 16c) and H = 120 m (Fig. 16d). All examined
4 pipelines are pressurized at a pressure level p = 8 MPa. In most of examined cases, higher p-
5 $values$ are reported for 'perfect' pipelines (i.e. w/t = 0), which generally exhibit a more 'elastic'
6 axial response for a given ground deformation compared to the equivalent imperfect pipelines
7 (i.e. w/t = 0.1). Similarly, higher p-$values$ are reported for pipelines embedded in trench TA,
8 compared to equivalent pipelines embedded in trench TB. Regardless of the effects of the
9 above parameters, the highest p-$values$ are reported for PGV_1 followed by PGV_2. On the
10 contrary the lowest values are found for PGA_1 and PGA_2.
11 Fig. 17 compares p-$values$ computed for X60 D = 914.4 mm 'perfect' (i.e. w/t = 0) and
12 'imperfect' (i.e. w/t = 0.1) pipelines embedded at diverse burial depths (i.e. h = 1.0 m or 2.0 m)
13 in trench TA in soil deposits with depth H = 60 m. The pipelines are pressurized at a pressure
14 level p = 8 MPa. The higher embedment of the pipeline seems to lead in higher p-$values$ for
15 some of the tested seismic IMs (i.e. PGA_r, PGA_1, PGA_2), compared to those computed for
16 equivalent pipelines embedded in shallower depth (i.e. h = 1.0 m). However, for other
17 measures, a higher embedment lead to either comparable or reduced p-$values$, compared to
18 those referring to shallower equivalent pipelines (e.g. PGV_1, PGV_2, PGD_1, PGD_2 etc).
19 Regardless of the above deviations, PGV_1 is again found to provide the highest p-$values$.
20 Fig. 18a compares p-$values$ computed for all tested seismic IMs in case of the D = 406.4 mm
21 pipelines examined herein. The p-$values$ refer to perfect (w/t = 0) and imperfect (w/t = 0.1)
22 pipelines, embedded in trench TA or TB in soil deposits with depth H = 60 m and pressurized
23 at a pressure level p = 8 MPa. No clear trends may be identified in these cases, regarding the
24 effects of backfill properties, backfill-pipe interface characteristics, steel grade of the pipeline
25 and imperfections of the pipeline walls, on the computed p-$values$. However, higher p-$values$
26 are reported for PGV-based IMs (i.e. PGV_1, PGV_2, PGV_r), while the lowest values are again
27 reported for PGA-based IMs (i.e. PGA_1, PGA_2). The same observations are made by comparing
28 the p-$values$ computed for all tested seismic IMs in case of the D = 1219.2 mm pipelines,
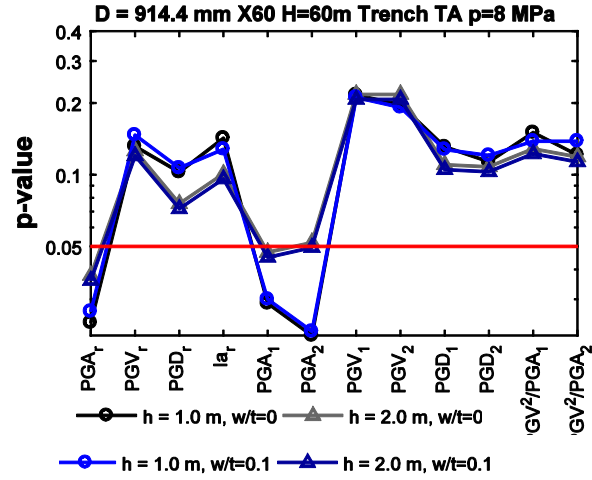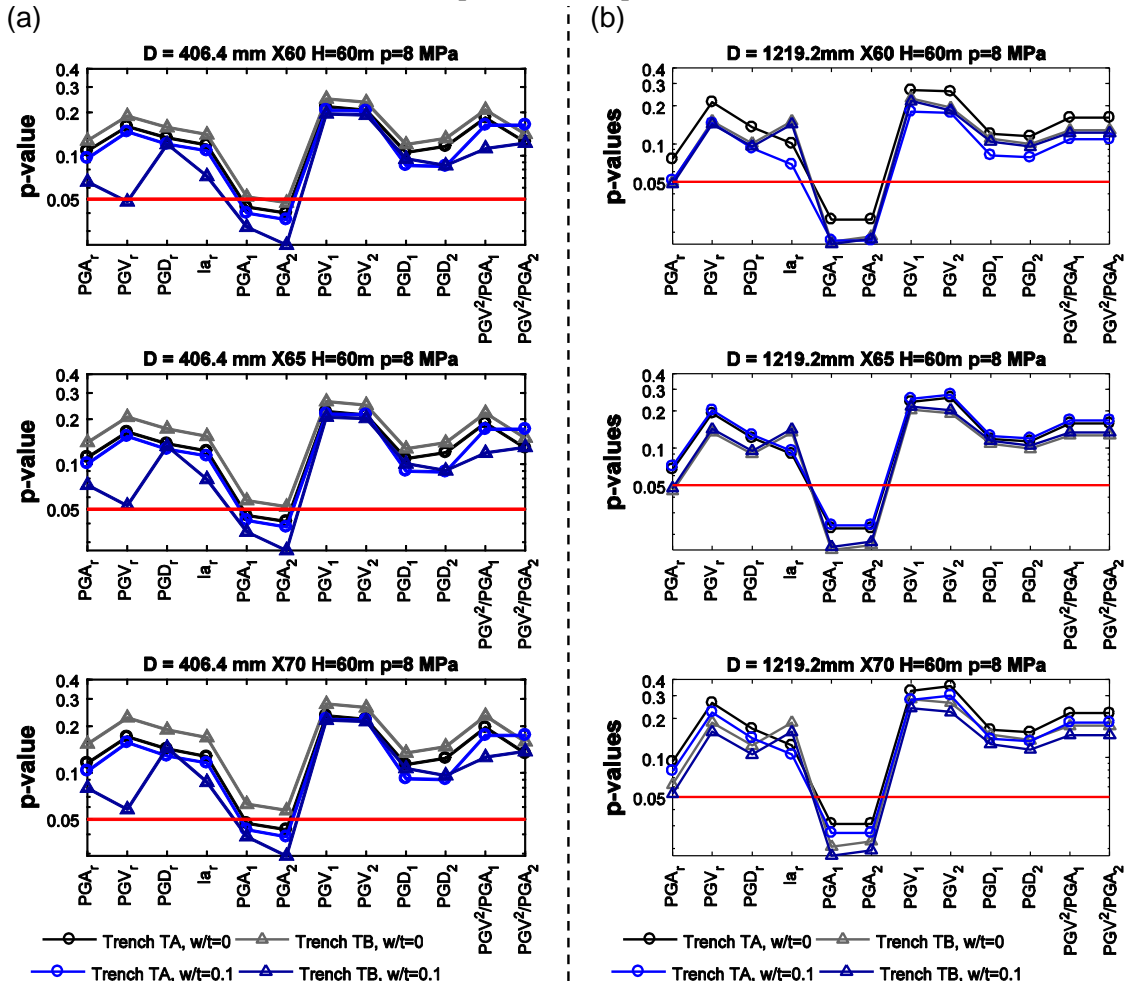29 examined herein (Fig. 18b).
30
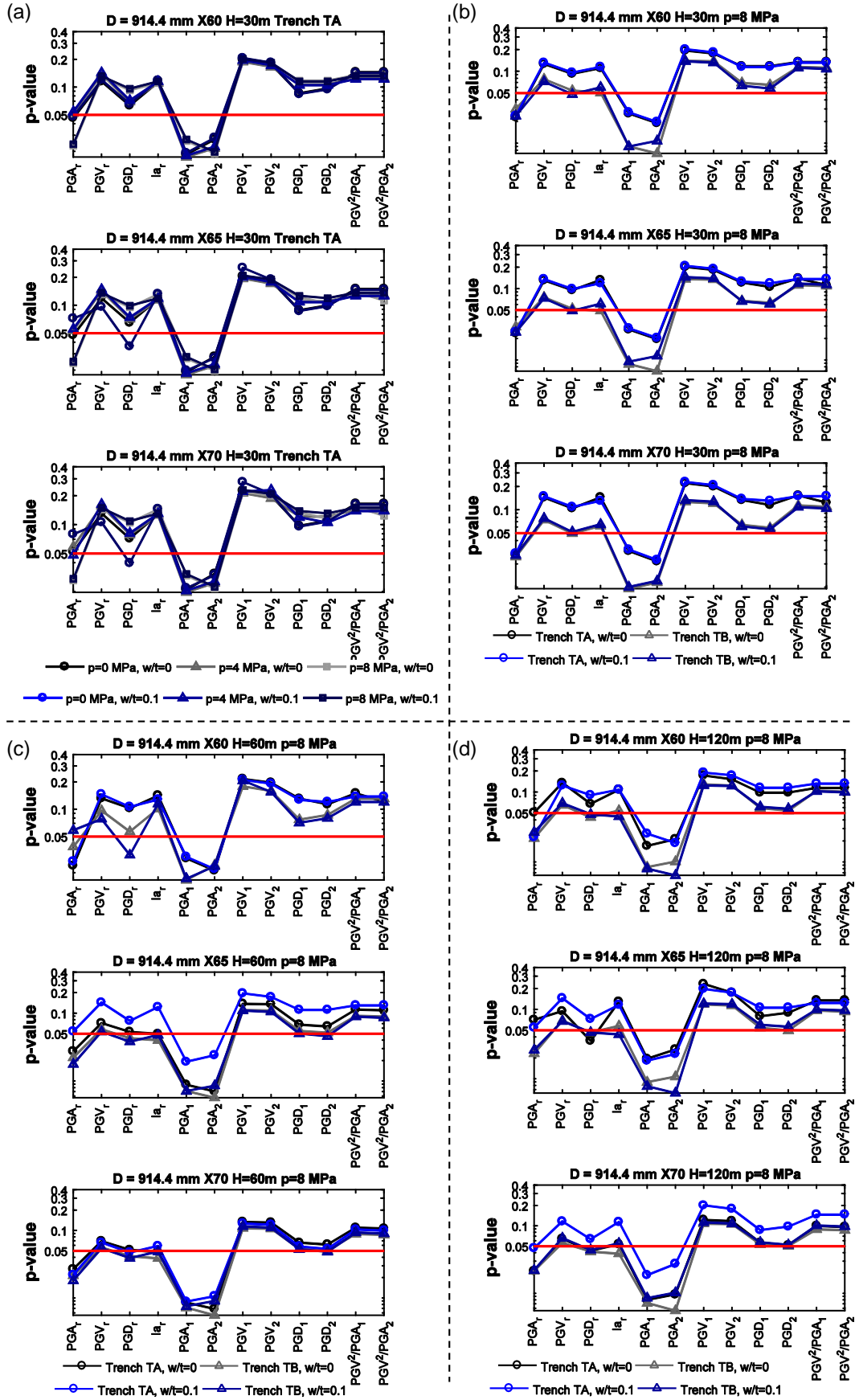
Fig. 16 Comparisons of *p-values* computed for all tested seismic *IMs* through regression analyses of $\varepsilon_{res}|IM$ relative to magnitudes (*M*) of the selected ground motions. (a) Effects of internal pressure *p*

1 and pipeline wall imperfections (*w/t*) on *p-values*. (b) Effects of trench properties and soil-pipe interface
2 characteristics on *p-values*. (c, d) Effect of soil deposit depth *H* on *p-values* (results for *D* = 914.4mm
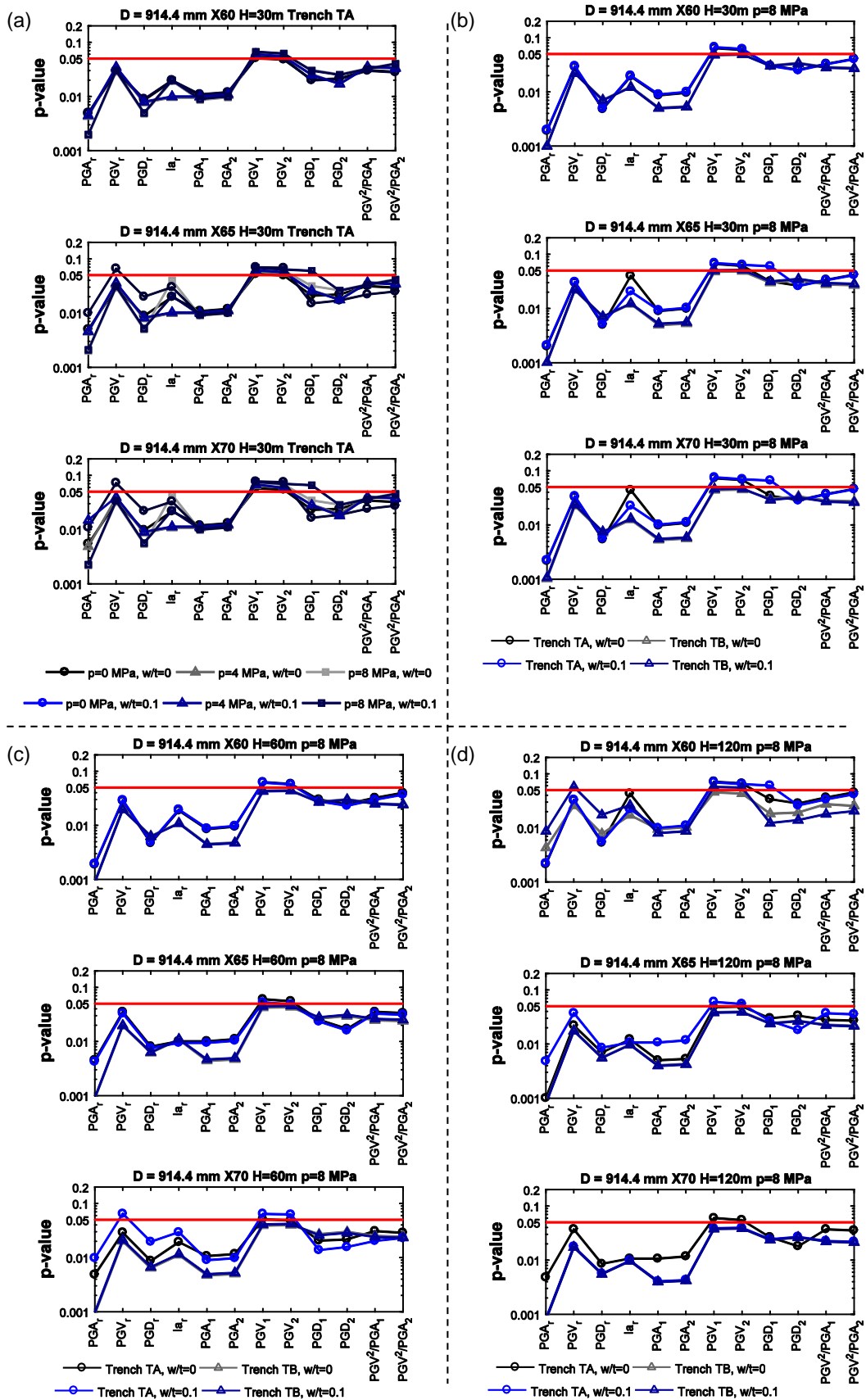3 pipelines).

4
5 **Fig. 17** Effect of burial depth *h* of the pipeline on *p-values* computed through regression analyses of
6 $\varepsilon_{res}\big|IM$ relative to magnitudes (*M*) of the selected ground motions. Results for X60 *D* = 914.4 mm
7 pipelines embedded in trench TA in soil deposits with depth *H* = 60 m.
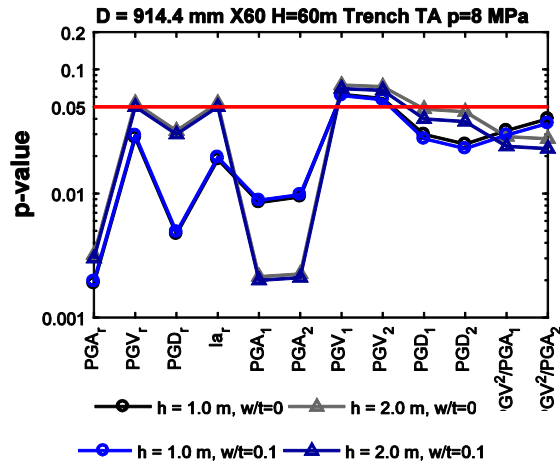
(a)   (b)

8
9 **Fig. 18** Comparisons of *p-values* computed for (a) *D* = 406.4 mm and (b) *D* = 1219.2 mm pipelines
10 through regression analyses of $\varepsilon_{res}\big|IM$ relative to magnitudes (*M*) of selected ground motions.

Figs. 19-21 summarize comparisons of *p-values* computed for all tested seismic *IMs* in all examined cases, based on regression analyses of the residuals of the compression axial strain ε of the pipeline ($\varepsilon_{res}|IM$) relative to the epicentral distance of the selected seismic records. More specifically, Fig. 19a summarizes *p-values* referring to X60, X65 or X70 $D = 914.4$ mm 'perfect' (i.e. *w/t* =0) or imperfect (i.e. *w/t* =0.1) pipelines, pressurized at various levels of pressure ($p = 0$, 4, 8 MPa) and embedded at a burial depth $h = 1.0$ in trench TA in soil deposits with depth $H = 30$ m. Lower *p-values* are generally computed here, compared to those predicted from regression analyses of the residuals of the compression axial strain ε of the pipeline ($\varepsilon_{res}|IM$) relative to the magnitudes of the selected seismic records. Additionally, in most of examined cases the computed *p-values* are found to be lower than the threshold of 0.05, indicating insufficiency of the tested *IMs*. However, the computed *p-values* for PGV_1 and PGV_2 are always slightly higher or higher than 0.05. Similar observations are made by comparing the computed *p-values* for all tested seismic *IMs,* in cases where the examined pipelines ($D = 914.4$ mm 'perfect' or imperfect pipelines) are embedded at a burial depth $h = 1.0$ in either trench TA or TB in soil deposits of depth $H = 30$ m (Fig. 19b), $H = 60$ m (Fig. 19c) and $H = 120$ m (Fig. 19d). The highest *p-values* are reported for PGV_1 followed by PGV_2. On the contrary the lowest values are found for PGA_r. PGV_1 reveals the highest *p*-value compared to other tested seismic *IMs*, even when the examined $D = 914.4$ mm pipeline is embedded deeper (i.e. at $h = 2.0$ m) (Fig. 20).

Fig. 21a compares *p-values* computed for all tested seismic *IMs* in case of X60, X65 and X70 $D = 406.4$ mm pipelines, based on regression analyses of the residuals of the compression axial strain ε of the pipeline ($\varepsilon_{res}|IM$) relative to the epicentral distance of the selected seismic records. The results refer to both 'perfect' (*w/t* = 0) and imperfect (*w/t* = 0.1) pipelines, pressurized at a pressure level $p = 8$ MPa and embedded in trench TA or TB in diverse soil deposits with depth $H = 60$ m. The trends regarding the effects of backfill properties, backfill-pipe interface characteristics, steel grade of the pipeline and imperfections of the pipeline walls, on the computed *p-values* are again not clear in these cases. Higher *p-values* are reported for PGV_1, PGV_2 and PGV_r. On the contrary, the lowest values are again reported for *PGA*-based measures. The same observations are made by comparing the *p-values* computed for all tested seismic *IMs*, in case of the $D = 1219.2$ mm pipelines examined herein (Fig. 21b).

Based on the discussion made above, PGV_1 is found to satisfy the sufficiency criterion in a mathematically rigorous way.

1
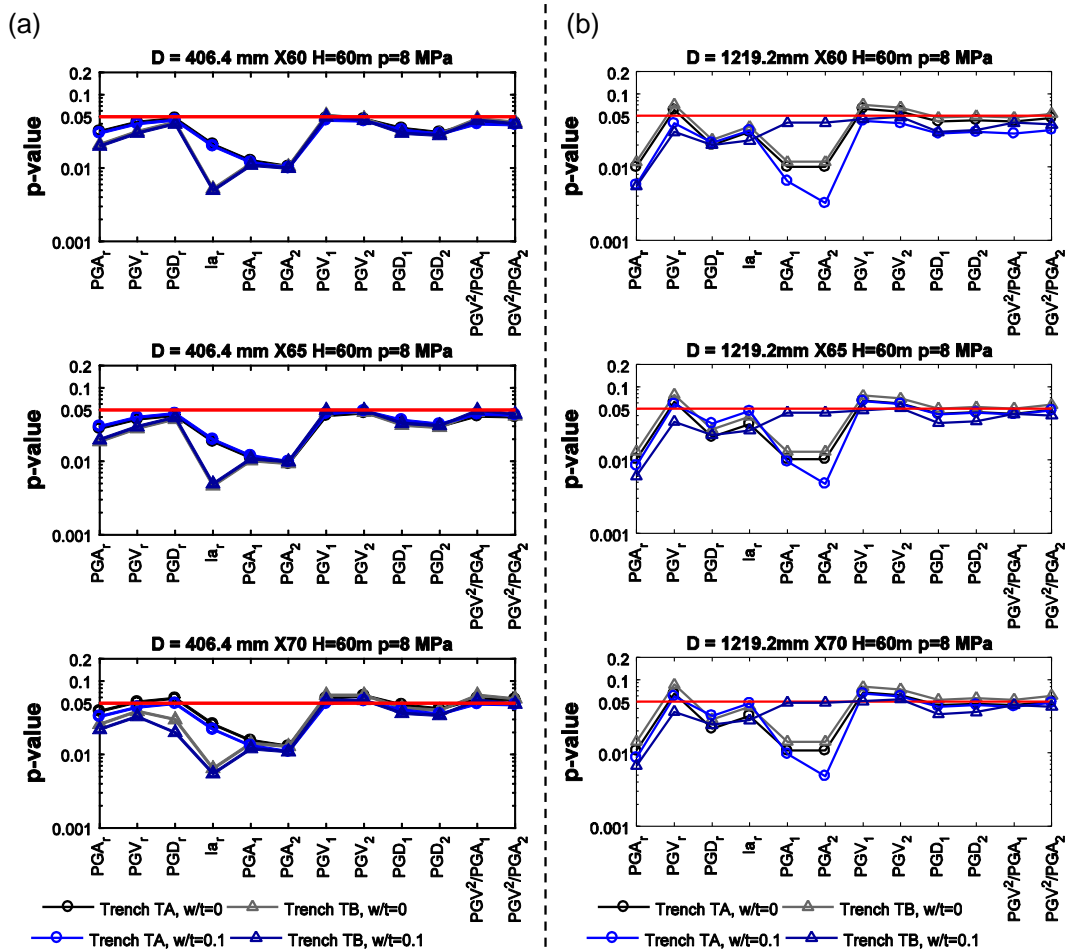2 **Fig. 19** Comparisons of *p-values* computed for all tested seismic *IMs* through regression analyses of
3 $\varepsilon_{res}\big|IM$ relative to epicentral distances $(\ln(R))$ of the selected ground motions. (a) Effects of internal
4 pressure *p* and pipeline wall imperfections (*w/t*) on *p-values*. (b) Effects of trench properties and soil-

1 pipe interface characteristics on *p-values*, (c, d) Effect of soil deposit depth *H* on *p-values* (results for *D*
2 = 914.4 mm pipelines).

3
4 **Fig. 20** Effect of burial depth, *h*, of the pipeline on *p-values* computed through regression analyses of
5 $\varepsilon_{res}|IM$ relative to epicentral distances (ln(*R*)) of the selected ground motions. Results for X60 *D* =
6 914.4 mm pipelines embedded in trench TA in soil subdeposits with depth *H* = 60 m.

7
8 **Fig. 21** Comparisons of *p-values* computed for (a) *D* = 406.4 mm and (b) *D* = 1219.2 mm pipelines
9 based on regression analyses of $\varepsilon_{res}|IM$ relative to epicentral distances (ln(*R*)) of the selected ground
10 motions.
11

5. Conclusions

This study examined the efficiency and sufficiency of various seismic *IMs* for the structural assessment of buried steel natural gas (NG) pipelines subjected to axial compression strains, the latter developed as a result of seismically-induced differential ground movement near geotechnical discontinuities. A de-coupled numerical framework was developed for this purpose, including a 3D soil-pipe numerical model, to rigorously evaluate the pipeline axial response, accounting for the soil-pipe interaction phenomena, and 1D soil response analyses that were used to determine critical ground deformation patterns at the geotechnical discontinuity, caused by ground shaking. A comprehensive numerical parametric study was performed for an ensemble of seismic records, considering critical parameters that control the axial response of buried steel NG pipelines, such as the dimensions of the pipeline, the pressurization level of the pipeline, potential geometric imperfections of the pipeline walls, the backfill and soil properties and the backfill-pipeline interface characteristics. The peak compression strain of the pipeline, ε, computed at the location of the assumed geotechnical discontinuity, was used as *EDP* to quantify the efficiency and sufficiency of the selected seismic *IMs* on the basis of regression analyses of this parameter, relative to the tested *IMs*. The main conclusions of the study are summarized in the following:

- The regression analyses of the peak compression strain of the pipeline, ε, relative to the peak ground velocity *PGV,* computed at ground surface as the maximum value of the peak velocities of the adjacent soil subdeposits, i.e. *PGV$_1$*, revealed the lowest standard deviations σ, regardless of the ground characteristics and pipeline dimensions. On the contrary, the regression analyses of the peak compression strain of the pipeline ε relative to *PGA-based IMs* revealed the highest standard deviations σ. Additionally, the regression analyses of the peak compression strain of the pipeline, ε, relative to *PGD* and *PGV^2/PGA* revealed higher standard deviations σ compared to *PGV*. Therefore, *PGV$_1$* found to be the most *efficient* intensity measure for the structural assessment of buried steel NG pipelines, crossing similar sites we those examined herein and subjected to seismically-induced axial ground deformations.

- The regression analyses of the residuals $\varepsilon_{res}|IM$ relative to the magnitude (*M*) and the epicentral distance (ln(*R*)) of the selected records, revealed the highest *p-values* for peak ground velocity *PGV* computed at ground surface as the maximum value of the peak velocities of the adjacent soil subdeposits, i.e. *PGV$_1$*. This observation indicates that this *IM* satisfies the sufficiency criterion in a mathematically rigorous way. On the contrary, *PGA-based IMs* where found to be the most inefficient ones.

Summarizing, *PGV$_1$* was found to be the optimum seismic *IM* for the structural assessment of buried steel NG pipelines, crossing geotechnical discontinuities, when subjected to seismically-induced axial ground deformations. This observation is in line with the theoretically expected superiority of *PGV*. Indeed, *PGV*, is directly associated with the longitudinal ground strains, which constitute the main loading mechanism of this infrastructure during ground shaking. This study constitutes a comprehensive numerical effort towards proving superiority of *PGV* as optimal seismic *IM* for the assessment of buried NG pipelines.

Acknowledgements

References

1. Chen WW, Shih BJ, Wu CW, Chen YC. Natural gas pipeline system damages in the Ji-Ji earthquake (The City of Nantou). In: Proc of the 6th international conf on seismic zonation; 2000.

2. Lee D-H, Kim BH, Lee H, Kong JS. Seismic behavior of a buried gas pipeline under earthquake excitations. Eng Struct 2009;31:1011-1023.

3. EQE summary report. The January 17. 1995 Kobe earthquake. EQE International;1995.

4. Scawthorn C, Yanev PI. Preliminary report 17 January 1995, Hyogo–ken Nambu, Japan earthquake. Eng Struct 1995;17(3):146-157.

5. O'Rourke MJ, Liu X. Response of buried pipelines subjected to earthquake effects. University of Buffalo, USA;1999.

6. Lanzano G, Salzano E, Santucci de Magistris F, Fabbrocino G. Seismic vulnerability of natural gas pipelines. Reliability Eng System Safety 2013;117:73-80.

7. Lanzano G, Salzano E, Santucci de Magistris F, Fabbrocino G. Seismic vulnerability of gas and liquid buried pipelines, J Loss Prev Process Ind 2014;28:72-78.

8. Lanzano G, Santucci de Magistris F, Fabbrocino G, Salzano E. Seismic damage to pipelines in the framework of Na-Tech risk assessment. J Loss Prevention Process Ind 2015;33:159-172.

9. Housner GW, Jenningst PC. The San Fernando California earthquake. Earthq Eng Struct Dyn 1972;1:5-31.

10. O'Rourke TD, Palmer MC. The Northridge, California Earthquake of January 17, 1994: Performance of gas transmission pipelines. Technical Report NCEER-94-0011. National Center for Earthquake Engineering Research. State University of New York at Buffalo, USA;1998.

11. O'Rourke MJ. Wave propagation damage to continuous pipe. Technical Council Lifeline Earthquake Engineering Conference (TCLEE), Oakland, CA, June 28-July 1, Reston, VA, American Society of Civil Engineers, USA;2009.

12. Karamitros DK, Bouckovalas GD, Kouretzis GP. Stress analysis of buried steel pipelines at strike-slip fault crossings. Soil Dyn Earthq Eng 2007;27:200-211.

13. Karamitros D, Zoupantis C, Bouckovalas GD. Buried pipelines with bends: analytical verification against permanent ground displacements. Can Geotech J 2013;53(11):1782-1793.

14. Vazouras P, Karamanos SA, Dakoulas P. Finite element analysis of buried steel pipelines under strike-slip fault displacements. Soil Dyn Earthq Eng 2010;30:1361-1376.

15. Vazouras P, Karamanos SA, Dakoulas P. Mechanical behavior of buried steel pipes crossing active strike-slip faults. Soil Dyn Earthq Eng 2012;41:164-180.

16. Vazouras P, Dakoulas P, Karamanos SA. Pipe-soil interaction and pipeline performance under strike-slip fault movements. Soil Dyn Earthq Eng 2015;72: 48-65.

17. Vazouras P, Karamanos SA. Structural behavior of buried pipe bends and their effect on pipeline response in fault crossing areas. Bull Earthq Eng 2017;15(11):4999-5024.

18. Melissianos V, Vamvatsikos D, Gantes C. Performance-based assessment of protection measures for buried pipes at strike-slip fault crossings. Soil Dyn Earthq Eng 2017a;101:1-11.

19. Melissianos V, Lignos X, Bachas KK, Gantes C. Experimental investigation of pipes with flexible joints under fault rupture. J Construct Steel Res 2017b;128:633-648.

20. Melissianos V, Vamvatsikos D, Gantes C. Performance assessment of buried pipelines at fault crossings. Earthq Spectra 2017c;33(1):201-218.

21. Sarvanis G, Karamanos S, Vazouras P, Mecozzi E, Lucci A, Dakoulas P. Permanent earthquake-induced actions in buried pipelines: Numerical modeling and experimental verification. Earthq Eng Struct Dyn 2018;47(4):966-987.

22. Demirci HE, Bhattacharya S, Karamitros D, Alexander N. Experimental and numerical modelling of buried pipelines crossing reverse faults. Soil Dyn Earthq Eng. 2018;114:198-214.

23. Tsatsis A, Gelagoti F, Gazetas G. Performance of a buried pipeline along the dip of a slope experiencing accidental sliding. Géotechnique 2018;68(11):968-988.

24. Psyrras N, Sextos A. Safety of buried steel natural gas pipelines under earthquake-induced ground shaking. A review. Soil Dyn Earthq Eng 2018;106: 254-277.

25. Psyrras N, Kwon O, Gerasimidis S, Sextos A. Can a buried gas pipeline experience local buckling during earthquake ground shaking? Soil Dyn Earthq Eng 2019;116:511-529.

26. Baker JW, Cornell CA. A vector-valued ground motion intensity measure consisting of spectral acceleration and epsilon. Earthq Eng Struct Dyn 2005;34:1193-1217.

27. Shome N, Cornell CA, Bazzurro P, Carballo JE. Earthquakes, records, and nonlinear responses. Earthq Spectra 1998;14:469-500.

28. Luco N, Cornell CA. Structure-specific scalar intensity measures for near-source and ordinary earthquake ground motions. Earthq Spectra 2007;232:357-392.

29. Cornell CA, Krawinkler H. Progress and challenges in seismic performance assessment. PEER Center News. 2000;32:1-4.

30. Mackie K, Stojadinovic B. Seismic demands for performance-based design of bridges. In: PEER Report 2003/16, University of California, Berkeley, CA; 2003.

31. Vamvatsikos D, Cornell CA. Developing efficient scalar and vector intensity measures for IDA capacity estimation by incorporating elastic spectral shape information. Earthq Eng Struct Dyn 2005;34:1573-1600.

32. Padgett JE, DesRoches R. Methodology for the development of analytical fragility curves for retrofitted bridges. Earthq Eng Struct Dyn 2008;37:1157-1174.

33. Padgett JE, Nielson BG, DesRoches R. Selection of optimal intensity measures in probabilistic seismic demand models of highway bridge portfolios. Earthq Eng Struct Dyn 2008;37:711-725.

34. Yang D, Pan J, Li G. Non-structure-specific intensity measure parameters and characteristic period of near-fault ground motions. Earthq Eng Struct Dyn 2009;38:1257-1280.

35. Kostinakis K, Athanatopoulou A, Morfidis K. Correlation between ground motion intensity measures and seismic damage of 3D RC buildings. Eng Struct 2015;82:151-167.

36. Fotopoulou S, Pitilakis K. Predictive relationships for seismically induced slope displacements using numerical analysis results. Bull Earthq Eng 2015;13(11):3207-3238.

37. Shakib H, Jahangiri V. Intensity measures for the assessment of the seismic response of buried steel pipelines. Bull Earthq Eng 2018;14(4):1265-1284.

38. American Lifelines Alliance (ALA). Seismic fragility formulations for water systems. Part 1-Guidelines. ASCE-FEMA, Washington, DC, USA; 2001.

39. Seed HB, Idriss IM. Soil moduli and damping factors for dynamic response analyses. Berkeley, California: College of Engineering, University of California; 1970.

40. European Committee for Standardization (CEN). EN 1998-1: Design of structures for earthquake resistance. Part 1: General Rules, Seismic Actions and Rules for Buildings, European Committee for Standardization, Brussels, Belgium; 2004.

41. Darendeli M. Development of a new family of normalized modulus reduction and material damping curves. Ph.D. Dissertation, University of Texas, Austin; 2001.

42. O'Rourke MJ, Hmadi K. Analysis of continuous buried pipelines for seismic wave effects. Earthq Eng Struct Dyn 1988;16:917-929.

43. ABAQUS. ABAQUS: theory and analysis user's manual version 6.12. Providence, RI, USA: Dassault Systemes Simulia; 2012.

44. Yun H, Kyriakides S. On the beam and shell modes of buckling of buried pipelines. Soil Dyn Earthq Eng 1990;9:179-193.

45. Paquette JA, Kyriakides S. Plastic buckling of tubes under axial compression and internal pressure. Intern J Mech Sci 2006;48:855-867.

46. Kyriakides S, Corona E. Plastic buckling and collapse under axial compression. Mechanical Offshore Pipelines Buckling Collapse, Vol. I, Elsevier Science, New York; 2007, p.280-318.

47. Tsinidis G, Di Sarno L, Sextos A, Psyrras N, Furtner P. On the numerical simulation of the response of gas pipelines under compression. In proc: 9th International Conference on Advances in Steel Structures, ICASS'2018, 5-7 Dec 2018, Hong Kong, China; 2018.

48. Tsinidis G, Di Sarno L, Sextos A, Furtner P. A critical review on the vulnerability assessment of natural gas pipelines subjected to seismic wave propagation. Part 2: Pipe analysis aspects. Tunnel Undergr Space Tech 2019a;92:103056.

49. Timoshenko SP, Gere JM. Theory of elastic stability. McGraw-Hill; 1961.

50. ArcelorMittal. High yield SAW welded Pipe API 5L grade X65 PSL 2;65:5-6; 2018.

51. Hashash YMA, Musgrove MI, Harmon JA, Groholski DR, Phillips CA, Park D. DEEPSOIL 6.1, User Manual. USA; 2016.

52. Hashash YMA, Park D. Viscous damping formulation and high frequency motion propagation in non-linear site response analysis. Soil Dyn Earthq Eng 2002;22(7):611-624.

53. Paolucci R, Pitilakis K. Seismic risk assessment of underground structures under transient ground deformations. Pitilakis K (ed) Earthquake Geotechnical Engineering. Geotech, Geol Earthq Eng, Springer;2007, p. 433-459.

54. Giardini et al.Seismic Hazard Harmonization in Europe (SHARE): Online Data Resource, doi: 10.12686/SED-00000001-SHARE; 2013.

55. Katsanos EI, Sextos A. Structure-specific selection of earthquake ground motions for the reliable design and assessment of structures. Bull Earthq Eng 2018;16(2):583-611.

56. Katsanos EI, Sextos A, Manolis G. Selection of earthquake ground motion records: A state-of-the-art review from a structural engineering perspective: Soil Dyn Earthq Eng 2010;30(4):157-169.

57. Moschen L, Medina RA, Adam C. A ground motion record selection approach based on multiobjective optimization: J Earthq Eng 2019;23(4):669-687.

58. Mergos P, Sextos A Selection of earthquake ground motions for multiple objectives using genetic algorithms: Eng Struct 2019;187:414-427.

59. Hashash YMA, Hook JJ, Schmidt B, Yao JI-C. Seismic design and analysis of underground structures. Tun Undergr Space Tech 2001;16 (2):247-293.

60. Pitilakis K, Tsinidis G. Performance and seismic design of underground structures, in: Maugeri, M., Soccodato, C. (Eds.), Earthquake geotechnical engineering design, Geotechnical Geological and Earthquake Engineering 2014; 28. Springer international publishing, Switzerland, pp. 279-340.

61. Tsinidis G, Di Sarno L, Sextos A, Furtner P. A critical review on the vulnerability assessment of natural gas pipelines subjected to seismic wave propagation. Part 1: Fragility relations and implemented seismic intensity measures. Tunnel Undergr Space Tech 2019b;86:279-296.

62. Gehl P, Desramaut N, Reveillere A, Modaressi H. Fragility functions of gas and oil networks. In: Pitilakis K, Crowley H, Kaynia A (eds) SYNER-G: Typology definition and fragility functions for physical elements at seismic risk, Geotech Geolog Earthq Eng 27, Springer; 2014, p.187-220.

63. Eguchi RT. Seismic vulnerability models for underground pipes. Proceedings of Earthquake Behavior and Safety of Oil and Gas Storage Facilities, Buried Pipelines and Equipment, PVP-77, ASME, New York, 368-373; 1983.

64. Ballantyne DB, Berg E, Kennedy J, Reneau R, Wu D. Earthquake loss estimation modeling for the Seattle water systems: Report to US Geological Survey under Grant 14-08-0001-G1526. Technical Report, Kennedy/Jenks/Chilton, Federal Way, Washington, USA; 1990.

65. Eguchi RT. Seismic hazard input for lifeline systems. Struct Saf 1991;10:193-198.

66. O'Rourke TD, Steward HE, Gowdy TE, Pease JW. Lifeline and geotechnical aspects of the 1989 Loma Prieta earthquake. Proceedings of the Second International Conference on Recent Advances in Geotechnical Earthquake Engineering and Soil Dynamics, St. Louis, MO, 1601-1612;1991.

67. O'Rourke TD, Toprak S, Sano Y. Factors affecting water supply damage caused by the Northridge earthquake. In: proc 6th US national Conference on Earthquake Engineering. EERI;1998.

68. Katayama T, Kubo K, Sato N. Earthquake damage to water and gas distribution systems. Proceedings of the U.S. In: proc of the National Conference of Earthquake Engineering, Oakland, CA: EERI;1979 p. 396-405.

69. Isoyama R, Katayama T. Reliability evaluation of water supply system during earthquakes. Report of the Institute of Industrial science, University of Tokyo, 30 (1); 1982.

70. Chen W, Shih BJ, Chen YC, Hung JH, Hwang H. Seismic response of natural gas and water pipelines in the Ji-Ji earthquake. Soil Dyn Earthq Eng 2002;22:1209-1214.

71. Barenberg ME. Correlation of pipeline damage with ground motions. J Geotech Eng ASCE, 1988;114(6):706-711.

72. O'Rourke MJ, Ayala G. Pipeline damage due to wave propagation. J Geotech Eng 1993;119(9):1490-1498.

73. Eidinger J, Maison B, Lee D, Lau B. East Bay municipal district water distribution damage in 1989 Loma Prieta earthquake. In: proc 4th US Conference on Lifeline Earthquake Engineering, ASCE, TCLEE, Monograph 6, 240-24; 1995.

74. Eidinger J. Water distribution system. In: Anshel J Schiff (ed.) The Loma Prieta, California, Earthquake of October 17, 1989 – Lifelines. USGS Professional Paper 1552-A, US Government Printing Office, Washington, A 63-A78; 1998.

75. Jeon SS, O'Rourke TD. Northridge earthquake effects on pipelines and residential buildings. Bull Seismol Soc Amer 2005;95:294-318.

76. Isoyama R, Ishida E, Yune K, Shirozu T. Seismic damage estimation procedure for water supply pipelines. In: proc of the 12th World Conference on Earthquake Engineering, paper No. 1762; 2000.

77. O'Rourke MJ, Deyoe E. Seismic damage to segment buried pipe. Earthq Spectra 2004;20(4):1167-1183.

78. Pineda-Porras O, Ordaz M. Seismic vulnerability function for high diameter buried pipelines: Mexico City's primary water system case. Proceedings of the International Conference on Pipeline Engineering Constructions, 2:1145–1154; 2003.

79. O'Rourke M, Filipov E, Uçkan E. Towards robust fragility relations for buried segmented pipe in ground strain areas. Earthq Spectra 2015;31(3):1839-1858.

80. Pineda-Porras O, Ordaz M. A new seismic intensity parameter to estimate damage in buried pipelines due to seismic wave propagation. J Earthq Eng 2007;11(5):773-786.

81. Hwang H, Chiu Y-H, Chen WY, Shih BJ. Analysis of damage to steel gas pipelines caused by ground shaking effects during the Chi-Chi, Taiwan. Earthq Spectra 2004;20(4):1095-1110.

82. Lee DH, Kim BH, Jeong SH, Jeon JS, Lee TH. Seismic fragility analysis of a buried gas pipeline based on nonlinear time-history analysis. Intern J Steel Struct 2016;16(1):231-242.

83. Jahangiri V, Shakib H. Seismic risk assessment of buried steel gas pipelines under seismic wave propagation based on fragility analysis. Bull Earthq Eng 2018;16(3):1571-1605.

84. Giovenale P, Cornell AC, Esteva L. Comparing the adequacy of alternative ground motion intensity measures for the estimation of structural responses. Earthq Eng Struct Dyn 2004;33:951-979.

85. Cornell CA, Jalayer F, Hamburger RO, Foutch DA. Probabilistic basis for 2000 SAC federal emergency management agency steel moment frame guidelines. J Struct Eng 2002;128:526–533.

86. Bakalis, K., Kohrangi, M., Vamvatsikos, D. 2018. Seismic intensity measures for above-ground liquid storage tanks. Earthquake Engineering & Structural Dynamics 47(9):1844-1863

87. Kazantzi AK, Vamvatsikos D. Intensity measure selection for vulnerability studies of building classes. Earthq Eng Struct Dyn. 2015;44(15):2677-2694.